Bacterial cytoskeleton diversity: The structure, assembly and regulation of Alp7A reveal conserved mechanisms of actin-based plasmid segregation.

by

Natalie Ann Petek

DISSERTATION

Submitted in partial satisfaction of the requirements for the degree of

DOCTOR OF PHILOSOPHY

in

Biochemistry and Molecular Biology

in the

GRADUATE DIVISION

of the

UNIVERSITY OF CALIFORNIA, SAN FRANCISCO

Dedication

I dedicate this work to my parents, Joseph and Lacreshia Petek, who have unconditionally

loved and supported me in every single crazy passion I have chosen to pursue.

Acknowledgements

Contributions

Chapter 1

Chapter 2

 James Kraemer collected the initial diffraction data and advised on crystal screens, and solved the later Alp7A structures by molecular replacement. James Fraser together with Dyche Mullins performed the bioinformatic nucleotide conformation analysis, and facilitated the interaction with Frank DiMiao. Frank DiMaio computationally solved the original Alp7A structure. Jessica Polka and Justin Kollman performed the 2D EM averaging.

Chapter 3

Alan Derman and Jason Royal performed the in-vivo Alp7R experiments.

Chapter 4

This began as a final project for the Tetrad macromolecules course. The students participated in collecting analytical ultracentrifugation data were: Karen Cheng, Karen Ruiz, Aditya Anand, and Xiaowei Yan. Daniel Elnatan helped perform the SAXS experiments and did all of the SAXS analysis. Dyche also helped with the initial auc experiments.

Chapter 5

Abstract

Bacterial Actin-Like Proteins (ALPs) participate in many biologically, clinically and commercially important processes, including segregation of low-copy plasmids. To better understand the biochemical principles underlying plasmid DNA segregation we purified a recently discovered plasmid-segregating ALP, Alp7A, and studied its structure and self-assembly *in vitro*. Monomeric Alp7A has a uniquely low affinity for nucleotides, binding ATP 1,000,000-fold more weakly than eukaryotic actin. The atomic structure of Alp7A (solved to 2.4 A resolution by x-ray crystallography) revealed that the low nucleotide affinity correlates with a unique nucleotide conformation. Alp7A has a low rate of spontaneous nucleation and, at low concentrations (<11 µM), forms ephemeral and highly dynamic polymers. At higher concentrations these ephemeral polymers are stabilized by lateral association, forming large bundles which contain antiparallel filaments. The accessory factor, Alp7R, dramatically increases the nucleation rate of Alp7A filaments and decreases their propensity to bundle, making them behave much more like ParM filaments. These nucleation and stabilization activities of Alp7R occur both *in vitro* and *in vivo* and do not require DNA, neither *alp7C* or non-specific DNA.

Table of contents

List of Tables

List of Figures

Chapter 1:

Introduction to the diversity of Actin-like proteins

Actin is one of the most abundant and conserved eukaryotic proteins from yeast to humans. The conservation of eukaryotic actin is likely the result of strong selective pressure placed on it by the multitude of regulatory proteins that interact with it to ensure spacial, architectural and temporal regulation of filament formation. Within a single cell, actin is able to participate in processes as varied as phagocytosis, cytokinesis, and cell motility (Pollard, 2016). Bacterial actin-like proteins have developed a different means for overcoming the challenge of forming multiple types of actin networks within a single cell. ALPs participate in a multitude of biological functions including: scaffolding the cell well synthesis machinery (Jones *et al*, 2001; Garner *et al*, 2011; Domínguez-Escobar *et al*, 2011; van Teeffelen *et al*, 2011), organelle positioning (Komeili *et al*, 2006), DNA segregation (Becker *et al*, 2006; Gerdes *et al*, 2000; Derman *et al*, 2009), and coordination and localization of the cell division machinery (Donachie *et al*, 1979). Instead of utilizing regulatory factors, ALPs have structurally diverged to enable multiple different actins to coexist within a single cell - without the ability to copolymerize - so that their various cellular tasks can be efficiently achieved.

Unlike the other functionally similar groups of ALPs (ie. those involved in cytokinesis or cell wall synthesis), the ALPs involved in plasmid DNA segregation do not belong to a single family. ParM, AlfA, and psK41-Alp32 share less than 20% sequence similarity. For this reason we know very little about how DNA segregating ALPs are related, and what overall features are common to actin-based plasmid segregation systems. Recent biochemical reconstitutions of DNA

segregation systems suggest that disparate mechanisms exist to partition large low copy number plasmids in rod-shaped bacteria - both gram-negative and gram-positive. The two best-characterized actin based partitioning systems AlfA and ParM both confer stability to their host plasmid by distributing DNA throughout the cytoplasm (Campbell & Mullins, 2007; Polka *et al*, 2014), however ParM does this by forming a bipolar spindle comprised of two antiparallel filaments and driving plasmid towards opposite poles(Gayathri *et al*, 2012), while AlfA robustly forms large filament bundles and constantly distributes plasmids bidirectionally along the length of the bundles (Polka *et al*, 2014). Recently a new DNA segregating ALP, Alp7A, was discovered. While Alp7A shares some *in vivo* characteristics with ParM (ie. dynamic instability, bipolar spindle), Alp7A has a unique requirement for accessory factors for dynamic and efficient polymerization (Derman *et al*, 2009). This is the first description of a regulation factor for any of the known bacterial actin homologs as bacterial actins are thus far described as being intrinsically dynamic, utilizing nucleotide-binding and hydrolysis induced conformation changes to regulate filament assembly and disassembly.

Understanding the mechanism of this regulation has been the focus of my thesis research, while also structurally characterizing Alp7A to better understand how it relates to ALPs in general.

I first purified Alp7A and characterized it's nucleotide dependent polymerization. Alp7A forms large polymer bundles and has unusual requirements for polymerization, namely a very weak nucleotide binding affinity, and a critical concentration (concentration below which polymer is unlikely to form) above the cellular concentration of Alp7A. After much labor, I obtained the first crystal structure of Alp7A. Our structure verifies the actin homology of Alp7A, but has novel nucleotide-binding characteristics that at least partially explain it's low affinity NTPs.

I next purified the DNA binding protein Alp7R and showed that it disrupts the formation of Alp7A bundles. In addition to prevent lateral filament annealing, Alp7R nucleates Alp7A polymer assembly, while simultaneously depressing the critical concentration. From phosphate release, and data from a hydrolysis dead mutant of Alp7A it is clear that Alp7R stabilizes highly dynamic filaments against disassembly. Together these data change our view of what is happening with Alp7A *in vivo* and shed new light on the stabilization of dynamically unstable polymers.

REFERENCES:

Becker E, Herrera NC, Gunderson FQ, Derman AI, Dance AL, Sims J, Larsen RA & Pogliano J (2006) DNA segregation by the bacterial actin AlfA during Bacillus subtilis growth and development. *EMBO J* **25:** 5919–5931

Campbell CS & Mullins RD (2007) In vivo visualization of type II plasmid segregation: bacterial actin filaments pushing plasmids. *J. Cell Biol.* **179:** 1059–1066

Derman AI, Becker EC, Truong BD, Fujioka A, Tucey TM, Erb ML, Patterson PC & Pogliano J (2009) Phylogenetic analysis identifies many uncharacterized actin-like proteins (Alps) in bacteria: regulated polymerization, dynamic instability and treadmilling in Alp7A. *Mol. Microbiol.* **73:** 534–552

Domínguez-Escobar J, Chastanet A, Crevenna AH, Fromion V, Wedlich-Söldner R & Carballido-López R (2011) Processive movement of MreB-associated cell wall biosynthetic complexes in bacteria. *Science* **333:** 225–228

Donachie WD, Begg KJ, Lutkenhaus JF, Salmond GP, Martinez-Salas E & Vincente M (1979) Role of the ftsA gene product in control of Escherichia coli cell division. *J. Bacteriol.* **140:** 388–394

Garner EC, Bernard R, Wang W, Zhuang X, Rudner DZ & Mitchison T (2011) Coupled, circumferential motions of the cell wall synthesis machinery and MreB filaments in B. subtilis. *Science* **333:** 222–225

Gayathri P, Fujii T, Moller-Jensen J, van den Ent F, Namba K & Lowe J (2012) A Bipolar

Spindle of Antiparallel ParM Filaments Drives Bacterial Plasmid Segregation. *Science*

338: 1334–1337

Gerdes K, Moller-Jensen J & Bugge Jensen R (2000) Plasmid and chromosome partitioning:

surprises from phylogeny. *Mol. Microbiol.* **37:** 455–466

Jones LJ, Carballido-López R & Errington J (2001) Control of cell shape in bacteria: helical,

actin-like filaments in Bacillus subtilis. *Cell* **104:** 913–922

Komeili A, Li Z, Newman DK & Jensen GJ (2006) Magnetosomes are cell membrane

invaginations organized by the actin-like protein MamK. *Science* **311:** 242–245

Polka JK, Kollman JM & Mullins RD (2014) Accessory factors promote AlfA-dependent

plasmid segregation by regulating filament nucleation, disassembly, and bundling. *Proc.*

Natl. Acad. Sci. U.S.A. **111:** 2176–2181

Pollard TD (2016) Actin and Actin-Binding Proteins. *Cold Spring Harb Perspect Biol*

van Teeffelen S, Wang S, Furchtgott L, Huang KC, Wingreen NS, Shaevitz JW & Gitai Z (2011)

The bacterial actin MreB rotates, and rotation depends on cell-wall assembly.

Proceedings of the ...

Chapter 2:

Structural basis of high-energy nucleotide binding by actin-like protein Alp7A.

Natalie Petek, James Kramer, James S. Fraser, Frank DiMiao, David Baker, David A. Agard and R. Dyche Mullins.

ABSTRACT:

Actin-family proteins share one defining structural feature: a nucleotide- and cation-binding domain created from a set of common conserved residues. Homologous residues within this "actin fold" coordinate the bound nucleotide and catalyze its hydrolysis in all actin-family proteins studied to date. Our understanding of the structural and functional diversity of the actin family expanded dramatically with the recent discovery of bacterial Actin-Like Proteins (ALPs): polymer-forming molecules that support many biologically, clinically, and commercially important processes. Here we report that, despite containing the "actin fold" and exhibiting ATP- and GTP-dependent self-assembly, the bacterial ALP, Alp7A, has a uniquely low affinity for nucleotides, binding ATP 1,000-fold more weakly than previously studied bacterial ALPs and 1,000,000-fold more weakly than eukaryotic actin. To understand how Alp7A interacts with nucleotides, we used x-ray crystallography and newly developed methods for molecular replacement to solve its atomic structure with a resolution of 2.2 Å. This structure revealed a bound nucleotide in a unique, high-energy conformation not found in any other member of the actin super-family (which includes actins, actin-related proteins, ALPs, HSP70s, and sugar kinases). This unique conformation is selected and stabilized by a network of conserved interactions at the heart of the actin fold. We propose that this low nucleotide affinity may reflect either genetic drift to the extreme functional limits of an ATPase, or an adaptive mechanism for storing energy required for rapid filament dynamics.

7

INTRODUCTION:

Bacteria and Archaea express polymer-forming proteins related to eukaryotic cytoskeletal proteins, actin. Actin-Like Proteins (ALPs) found in bacteria perform a plethora of cellular tasks including: cell wall assembly (Jones *et al*, 2001; Garner *et al*, 2011; Domínguez-Escobar *et al*, 2011; van Teeffelen *et al*, 2011), organelle positioning(Komeili *et al*, 2006), DNA segregation (Becker *et al*, 2006; Gerdes *et al*, 2000; Derman *et al*, 2009; Popp *et al*, 2010b), and cytokinesis (Donachie *et al*, 1979).

While ALPs contain the basic actin family architecture, they share very little overall sequence conservation with each other or eukaryotic actins (Bork *et al*, 1992). Additionally their self assembly properties and filament architecture vary significantly. The actin super-family of proteins is defined by a central nucleotide-binding domain comprising a small set of conserved residues, distributed across five sequence motifs. Beyond this relatively small number of conserved residues, the structure and function of actin super-family proteins varies significantly, from cytoskeletal elements to chaperones and sugar kinases (Bork *et al*, 1992).

Several low copy-number plasmids employ ALPs to ensure their survival within bacterial populations by actively dispersing plasmid DNA so that it is retained within a bacterial population. Actin-based plasmid-segregation operons encode both an actin-like protein and a DNA-protein complex that work together to promote plasmid inheritance. Polymerization of the actin-like protein generates force to move DNA through the cytoplasm, increasing the probability that both daughter cells will inherit at least one plasmid..

In the present study we describe the self-assembly of a plasmid-segregating actin-like protein, Alp7A, which shares less than 16% sequence identity with ParM and AlfA, two well characterized plasmid segregating ALPs. We show that similar to other bacterial actins (Popp *et al*, 2008; 2010a; Hara *et al*, 2007), Alp7A is capable of polymerizing in both ATP and GTP, and that it robustly forms bundles in with both nucleotides.

We show that Alp7A has a uniquely low affinity for nucleotides, binding ATP 1,000,000-fold more weakly than eukaryotic actin. From the atomic structure of Alp7A, determined by x-ray crystallography, we learn that this that low affinity for nucleotides reflects a preference for binding a rarely occurring nucleotide conformation. This low nucleotide affinity may reflect either genetic drift to the extreme functional limits of an ATPase, or an adaptive mechanism to ensure rapid nucleotide exchange or perhaps reduce cellular stress imposed by Alp7AR-containing plasmids.

RESULTS:

To understand how nucleotide-binding regulates self-assembly of Alp7A, we used electron microscopy and right-angle light scattering to characterize polymers formed by purified Alp7A under various buffer conditions. Similar to other bacterial and archaeal actin-like proteins (Popp *et al*, 2008; Polka *et al*, 2009; Hara *et al*, 2007), Alp7A forms polymers in both ATP and GTP (Figure 1A-E) In these experiments we noticed that Alp7A polymers formed in the presence of ATP consistently polymerize faster and (Figures 1D-E), have a much lower critical concentration (Figure 1F) in ATP-containing buffers (10.3 µM) compared to buffers containing GTP (14.9 µM)..

Unlike any previously studied actin or actin-like protein, purified Alp7A formed no detectable polymers in buffers with less than 1 mM ATP or GTP (figure 1G). This result was the first hint that Alp7A might have an exceptionally low affinity for nucleotides, and it was supported by the fact that we detected no binding of Alp7A to etheno-ATP, even when this fluorescent nucleotide analog was present at concentrations above 10 µM (unpublished observations). To estimate the affinity of Alp7A for ATP and GTP we resorted to nucleotide-dependent polymerization assays. Plots of steady-state light scattering intensity versus nucleotide concentration revealed that Alp7A binds ATP and GTP with approximately equal affinity (K_d ~2.5mM; Figure 1G). This affinity for ATP is 50,000-fold weaker than that of the bacterial protein ParM (42 nM) and 1,000,000-fold weaker than that of conventional eukaryotic actin (1.2nM), approaching the estimated concentration of ATP in bacterial cytoplasm (3-5 mM)(Buckstein *et al*, 2008).

To determine the ultrastructure of Alp7A polymers, we performed electron microscopy of negatively stained samples. In all buffer conditions that promote polymerization —as determined by light scattering and electron microscopy— we observed large, sheet-like bundles composed of numerous ~10 nm filaments arranged side-by-side. In two-dimensional averages, the filaments within a flattened bundle (Figure 1A, inset) sometimes appear to be polar, with an antiparallel orientation. We observed these flat polymer bundles under a myriad of pH, nucleotide, and ionic strength conditions, and we failed to find conditions that promote assembly of non-bundled Alp7A filaments. At protein concentrations close to the apparent critical concentration, Alp7A bundles appear as flattened ribbons that often twist (figures 1A-B, S1C-D). \ These twists occur with no consistent frequency or handedness (figures S1D-F). The width of Alp7A bundle is not fixed and increases in size with increasing protein concentrations (figures S1A-F)

The atomic structure of ADP-Alp7A

To understand the biophysical origin of its unique properties, we crystallized Alp7A and solved its atomic structure. In the presence of 10mM ADP, Alp7A formed crystals that diffracted well out to 2.3 Angstroms. We attempted to obtain experimental phases using Multi-wavelength Anomalous Dispersion (MAD) of seleno-methionine (SeMet) residues. Surprisingly, however, incorporation of SeMet into Alp7A rendered the protein incompetent for polymerization, a key step in its purification. Initial attempts to solve the structure of Alp7A by molecular replacement, using models based on conventional actin, ParM, MreB, or the archaeal actin Ta0583, also failed. We then tested search models created using subdomains from all existing structures of actins,

11

actin-like proteins, and Hsp70-family chaperones, and we finally solved the structure using MR-

Rosetta (Dimaio, 2013). Briefly, we generated ~1800 homology models by combining pieces

from 15 templates (1yuw 3gl1 3qfu 2e8a 3fe1 3i33 1jcf 2fsk 2zgy 1s3x 2fsj 3js6 1jce 2v7y

1mwk), searched against the Alp7A data, and retained the highest scoring molecular replacement

solution (TFZ=7, LLG=40). Although this initial solution did not yield maps that could be

automatically interpreted, rebuilding ~650 models into the density followed by refinement,

incorporating the Rosetta Energy Function and an electron density term, eventually yielded

interpretable maps. A combination of Rosetta-based real space refinement, Phenix Autobuild, and

conventional Phenix reciprocal space refinement(Terwilliger *et al*, 2012) enabled us to perform a

fully automated chain tracing of nearly the entire Alp7A molecule. All totaled, this strategy

required creation and analysis of more than 6000 test structures and used more than 3000 hours

of CPU time, making this one of the most computationally intensive protein structures solved to

date.

Consistent with low-affinity nucleotide binding, the first electron density map of Alp7A, solved

at 2.3Å resolution, contained little density for the bound nucleotide. To more fully populate the

nucleotide binding site, we soaked Alp7A crystals in increasing concentrations of ADP or AMP-

PNP. Crystals soaked in 10-30mM AMP-PNP dissolved, suggesting that this nucleotide analog

induced a significant conformational change in the protein. Crystals soaked in 40 mM ADP

produced maps with much more electron density in the nucleotide-binding pocket, with the

initial F_o-F_c displaying strong density for ADP (Figure 2B). In the end, we built our final Alp7A-

ADP model from a 2.2 Å data set collected from ADP-soaked crystals and solved by molecular replacement using the initial 2.3 Å model (Figure 2A).

Conservation of the actin fold

The atomic structure of Alp7A reveals why our initial attempts at molecular replacement failed to produce accurate phase information. In addition to low sequence identity with eukaryotic actins (~14%) and the actin-like protein ParM (~16%), the average RMS deviations of the Alp7A atomic structure from those of actin (1J6Z) and ParM (1MWM) are also quite large (9.74A and 5.75A respectively), underscoring the need for a novel molecular replacement strategy in the absence of experimentally determined phases. Compared to conventional actin, Alp7A represents the most structurally divergent actin-like protein studied to date.

While it diverges significantly from conventional actin, the atomic structure of Alp7A contains, at its heart, a recognizable actin fold. Like other actin-family members, Alp7A is a bi-lobed molecule, comprising two folded domains (I and II) connected by a flexible 'hinge' region. The space between the two large domains creates a deep, nucleotide-binding cleft. In eukaryotic actin, the central cleft is considered *closed* in the ATP bound state, when the distance between residues S14 and G158 is approximately 5.5 Å, and considered *open* in the nucleotide-free (apo) state, when the S14-G158 distance increases to 8.2 Å (Porta & Borgstahl, 2012). In ADP-Alp7A the equivalent reference distance for the central cleft (N12-G216) is 7.0 Å, similar to other bacterial actin-like proteins, which maintain a relatively open conformation even when bound to nucleotide (Table S2). The two large domains of Alp7A (Figure 2a) can be further divided into

four subdomains, analogous to those defined for conventional actin: Ia, Ib, IIa, and IIb.

Conserved structural elements in subdomains Ia and IIa form a pair of mirrored, five-stranded

beta sheets flanked by two or three alpha helices and —similar to conventional actin— residues

within these conserved motifs interact with the bound nucleotide (Figure 2a and 2b). Structural

elements in domains IIa and IIb vary significantly between different actin-like proteins, a

variability which likely contributes to the observed heterogeneity in the architecture of actin-like

filaments.

A two-residue "molecular filter" selects for high-energy nucleotide conformations

Although many nucleotide-coordinating residues are conserved (Figure 2D, 3A), the

conformation of ADP bound to Alp7A turns out to be highly atypical for an actin-family protein

(Figure 3A-B). Namely the adenine ring is strongly twisted relative to the ribose group, while the

ribose itself puckers in an unusual manner. To more easily compare the ADP in our Alp7A

structure with nucleotides bound to other proteins, we compiled all X-ray structures in the PDB

database [(www.rcsb.org](www.rcsb.org), (Berman *et al*, 2000)) that contained both a protein and an adenosine

nucleotide but no RNA or DNA. To ensure that we could accurately describe the conformation of

the nucleotide, we also limited our collection to structures with resolution of 2.5Å or higher. For

each protein-bound nucleotide we computed the base-ribose torsion angle and the ribose pucker

(Figure 4A). The base-ribose torsion angles (C4-N9-C1'-O4') of most protein-bound nucleotides

—including those bound to bacterial actin-like proteins, eukaryotic actin-related proteins, and

conventional actins— fall into a cluster centered around ~240 degrees. In contrast, the adenine of

ADP bound to Alp7A has a torsion angle of ~70 degrees, meaning that it is rotated almost 180

degrees away from its conformation in other actin-like proteins. Similarly, the ribose pucker of

Alp7A-bound ADP —described by the *pseudorotation* angle— falls outside the large cluster of

structures centered around 150 degrees (C2'-endo conformation) that contains most actins and

actin-like proteins, and instead clusters with a much smaller group of structures between 60-90

degrees (corresponding to O4-*endo* and *planar* conformations). Plotting the base-ribose torsion

angle and ribose pucker on a two-dimensional conformation map places the Alp7A-bound ADP

within a sparsely populated island of nucleotide conformations, composed of a variety of

unrelated proteins. Its relative rarity indicates that this nucleotide conformation represents a

short-lived, high-energy state: an interpretation that is consistent with a very slow association

rate constant and very weak nucleotide binding affinity (Figure 1B).

The structure of the nucleotide binding pocket reveals how Alp7A selects for such an unusual

nucleotide conformation. In actin and ParM, the adenosine of the bound nucleotide is

coordinated by conserved interactions with glycine residues in the 'adenine' loop in domain IIA

(Figure 2C-D, 3A-B), and non-conserved glutamic acids from domain IIA or IIB respectively

(Figure 3B). While the 'adenine loop' residues are conserved in Alp7A, the adenine ring of the

ADP is sandwiched in a pi-stack between residues Y271 and R363, from subdomains IIB and IA

respectively. In an overlay of Alp7A and Actin bound to ADP (1J6Z), Y271 of Alp7A protrudes

into the nucleotide binding pocket of actin and sterically clashes with the adenine moiety of

actin's bound nucleotide (Figure 3C-D). The orientation of the nucleotide-coordinating residues

of Alp7A and their position relative to the highly conserved network of interactions that position

the ribose (G329-G330), the phosphates (D9/G11 and D212/G214), as well as the bound

15

magnesium ion (E180A), creates a filter that rejects nucleotides with base-ribose dihedral angles

outside a narrow window around 73 degrees. The pi-stacking interaction that coordinates the

adenine moeity also facilitates an inter-helix salt bridge between R363 and E25 which appear to

stabilize the closed, polymerization competent, conformation of Alp7A.

Although nucleotide binding is weak and their conformation is unusual, several facts argue that

conventional nucleotides (ie. ATP and GTP) are the physiologically relevant substrates of Alp7A,

including: (i) they induce a polymerization-competent conformation of the Alp7A molecule; (ii)

conserved residues coordinate both the ribose and phosphate groups; and (ii) ATP is positioned

correctly for polymerization-induced nucleotide hydrolysis. Additionally, synthetic nucleotides

such as AMP-PNP, GMP-CPP, etheno-ATP, MANT-ATP, fail to induce polymerization or require

nucleotide concentrations above 30 mM to do so. This suggests to us that --often very small--

deviations from the standard nucleoside triphosphate structure are not tolerated, likely

eliminating rare cellular nucleotides as the substrate of Alp7A.

Divergent surface features in Alp7A

Our Alp7A structure also reveals two surface features that differ significantly from other actin-

family proteins: (1) the very long c-terminal α-helix that protrudes from domain Ia; and (2) the β-

barrel that runs from domain Ia into domain Ib and surrounds the conserved α-helix-3 (Figure

2A, 2C). The C-terminal helix is much longer than that found in actin or any actin-like protein of

known structure, projecting beyond the globular envelope of the protein to contact a monomer in

an adjacent 'protofilament' of the crystal lattice (Figure S3A-B). This suggested to us that the C-

16

terminal helix might play a role in filament-filament interaction, an idea supported by the fact

that another bacterial actin-like protein with a similar--albeit shorter-- C-terminal tail, Psk41/

Alp32, also forms ribbon-like bundles (Popp *et al*, 2010b). Truncations of the C-terminal tail that

abolish lateral protofilament contacts within the crystal lattice (Alp7A 1-383), however, had no

effect on bundling, or critical concentration (Figures S3C-G) while larger truncations in this

region destabilized the protein and rendered it insoluble. Uncovering the molecular determinants

of anti-parallel filament association will, therefore, likely require high-resolution electron

microscopy studies of Alp7A bundles. In addition, low-resolution projections of protofilaments

in the crystal lattice (Figure S2D) reveal that this helix falls between adjacent parallel

protofilaments, suggesting that the lateral interactions in the crystal lattice may not represent the

physiological structure. The β-barrel in domains Ia-Ib is not shared with eukaryotic actin —

whose domain Ib is more minimal— but partial β-barrels are found in other bacterial actin-like

proteins, including ParM (Figure 2A) and the archaeal actin Ta0583 (Figure S2A).

DISCUSSION:

Significance of Alp7A's low affinity for nucleotide

A defining feature of actin-like proteins [10] is a central cleft that binds nucleotide triphosphates. Alp7A requires nucleotide for polymerization but, remarkably, its affinity for nucleotide is 1,000,000-fold weaker ($K_d \sim$ mM) than that of conventional actin. Alp7A's low affinity for nucleotides may simply reflect genetic drift and the absence of selective pressure on high-affinity binding. That is, random mutations that decrease the affinity for nucleotide might have little effect on DNA segregation as long as the dissociation constant for ATP binding remains below the cellular concentration of ATP.. The pi-stacking conformation of the base in the binding pocket may reduce the specificity for a particular nucleoside triphosphate--as the interactions between protein and nucleotide do not rely on a particular functional group-- allowing for the binding of any available NTP. This would further diminishing the need for high-affinity binding as it effectively increases the cellular concentration of Alp7A substrate.

On the other hand, very weak nucleotide binding might serve a useful purpose, by shutting down the energy-consuming process of plasmid segregation in times of cellular stress. By reducing stress on bacterial hosts such a weak nucleotide binding might confer a selective advantage. Interestingly, ParM, which binds ATP with 1000-fold higher affinity than Alp7A, may have evolved a functionally similar mechanism to protect host cells. In this case, small amounts of ADP prevent ParM filament formation, even in high concentrations of ATP (Garner *et al*, 2004). We suspect that such "safety switches" generally reduce plasmid-induced stress under marginal growth conditions and may be a common feature of plasmid segregation systems. We aim to test this idea in future studies.

Finally, ultra-low affinity for ATP might be an epiphenomenon of the biophysical mechanism underlying rapid disassembly of Alp7A filaments. The nucleotide bound to Alp7A turns out to have a highly unusual conformation, a rarely occurring high-energy state that likely explains the exceptionally low affinity for nucleotide. Gayathri et al. (2013) proposed that strain in the ribose ring of the nucleotide bound to ParM might store energy that could be released by conformational changes in the protein that promote rapid filament disassembly (Gayathri *et al*, 2012). Such a mechanism might underlie rapid disassembly of Alp7A filaments. Additional structural and biophysical studies of dynamically unstable actin-like proteins will help clarify whether nucleotide conformation plays a general role in polymer destabilization. ParM and Alp7A share very little sequence homology and their bound nucleotides have very different conformations so, if both proteins use nucleotide conformation to store energy required for polymer disassembly, then the two proteins likely hit upon the same mechanism independently.

METHODS:

Expression and Purification of Alp7A

Alp7A was codon optimized (Mr. Gene) and cloned into the pet28a vector using the NcoI and HindIII restriction sites. Alp7A in Pet28 is freshly transformed for each purification into C43 cells and grown in TPM media at 37°C to an OD of 0.4-0.6, then shifted to 18°. Cultures were induced overnight with 0.2mM IPTG. Cultures were pelleted, then washed with 1x PBS. Washed pellets were flash frozen in liquid nitrogen and stored at -80°C.

To purify native Alp7A, three liters of expression culture were resuspended in Lysis buffer (25mM Tris pH 7.6, 100 mM KCl, 1mM EDTA, 1mM DTT, PMSF). Cells are dounce homogenized pri or to lysis by 3x passes through an Emulsiflex-C3 (Avestin).Lysates were cleared with a high-speed spin (60 min at 170,000×g, 4°C) to remove cellular debris and insoluble protein. Ammonium sulfate was added slowly to the cleared lysate to 50% solubility. Lysate is stirred at 4°C for one hour after all ammonium sulfate has been added. The precipitate is removed by centrifugation at 170,000xg for 30 minutes, 4°C. At this step Alp7A is in the soluble fraction; the supernatant was transferred to a clean ultracentrifuge tube and brought to room temperature using an ambient water bath. 5 mM ATP/6 mM MgCl$_2$ are then added to induce polymerization. After a 15 minute incubation, the polymer was pelleted by high speed centrifugation (20 min at 170,000×g, 25°C) and then resuspended in 1/10 volume of cold depolymerization buffer (25mM Tris pH 7.6, 200mM KCl, 6mM EDTA, 1mM DTT). The resuspended protein was dialyzed overnight to remove residual ATP and ensure complete depolymerization. Alp7A was gel filtered on Superdex S-200 resin into polymerization buffer

(25 mM Tris pH 7.6, 100 mM KCl, 1 mM $MgCl_2$, 1mM DTT); the purest protein fractions were pooled and dialyzed into storage buffer (polymerization buffer + 20% glycerol). Aliquots are snap frozen in liquid nitrogen and stored at -80°C. Protein is quantified by the Alp7A extinction coefficient $34,965M^{-1}cm^{-1}$.

Crystallization and Structure Determination

Crystals were grown by hanging drop/vapor diffusion in 4μl drops. Drops were composed of 1μl ~1mg/ml protein containing 10mM ADP, 1μl additive (Hampton Research Silver Bullets 22-HR2-996-22), and 2μl well solution (0.16 M magnesium acetate, 0.08 M sodium cacodylate pH 6.5, 16% w/v PEG 8000, 20% v/v glycerol). Protein Structure was solved as explained in part in the experimental procedures.

Molecular Replacement. using MR-Rosetta. Briefly, we generated ~1800 homology models by combining pieces from 15 templates (1yuw 3gl1 3qfu 2e8a 3fe1 3i33 1jcf 2fsk 2zgy 1s3x 2fsj 3js6 1jce 2v7y 1mwk), searched against the Alp7A data, and retained the highest scoring molecular replacement solution (TFZ=7, LLG=40). Although this solution did not initially yield maps that could be automatically interpreted, rebuilding ~650 models into the density followed by refinement incorporating the Rosetta Energy Function and an electron density term eventually yielded interpretable maps. A combination of Rosetta-based real space refinement, Phenix Autobuild, and conventional Phenix reciprocal space refinement (Dimaio, 2013) allowed for fully automated chain tracing of nearly the entire Alp7A molecule.

Analysis of the structure was performed using The PyMOL Molecular Graphics System (Version 1.6 Schrödinger LLC), and the UCSF Chimera Package (Pettersen *et al*, 2004). Figures were made using Pymol.

Negative Stain Electron Microscopy

Samples were prepared by applying 4ul of polymerization mix to 200mesh, Formvar carbon film coated, (Electron Microscopy Sciences-FCF200-Cu) glow discharged grids, and incubating for 30 seconds. Grids were washed 3x in buffer, blotting between washes. Grids were stained 3x with 0.75% uranyl formate, blotting between applications. The third stain step was done for 30 sec. Micrographs were taken with a Technai T12 microscope using an acceleration voltage of 120 kV and a magnification of x27,000 or x48,000. Images were recorded with a Gatan 4k x 4k charge-coupled device camera.

Right Angle Light Scattering

Light scattering experiments were performed using an ISS K2 fluorimeter at a wavelength of 320nm. Polymerization of Alp7A was induced by hand mixing with nucleotide $+ Mg^{++}$. For each condition four to five traces were background subtracted and averaged.

REFERENCES:

Becker E, Herrera NC, Gunderson FQ, Derman AI, Dance AL, Sims J, Larsen RA & Pogliano J
(2006) DNA segregation by the bacterial actin AlfA during Bacillus subtilis growth and
development. *EMBO J* **25:** 5919–5931

Berman HM, Westbrook J, Feng Z, Gilliland G, Bhat TN, Weissig H, Shindyalov IN & Bourne
PE (2000) The Protein Data Bank. *Nucleic Acids Res.* **28:** 235–242

Bork P, Sander C & Valencia A (1992) An ATPase domain common to prokaryotic cell cycle
proteins, sugar kinases, actin, and hsp70 heat shock proteins. *Proc. Natl. Acad. Sci.
U.S.A.* **89:** 7290–7294

Buckstein MH, He J & Rubin H (2008) Characterization of nucleotide pools as a function of
physiological state in Escherichia coli. *J. Bacteriol.* **190:** 718–726

Derman AI, Becker EC, Truong BD, Fujioka A, Tucey TM, Erb ML, Patterson PC & Pogliano J
(2009) Phylogenetic analysis identifies many uncharacterized actin-like proteins (Alps) in
bacteria: regulated polymerization, dynamic instability and treadmilling in Alp7A. *Mol.
Microbiol.* **73:** 534–552

Dimaio F (2013) Advances in Rosetta structure prediction for difficult molecular-replacement
problems. *Acta Crystallogr. D Biol. Crystallogr.* **69:** 2202–2208

Domínguez-Escobar J, Chastanet A, Crevenna AH, Fromion V, Wedlich-Söldner R & Carballido-López R (2011) Processive movement of MreB-associated cell wall biosynthetic complexes in bacteria. *Science* **333:** 225–228

Donachie WD, Begg KJ, Lutkenhaus JF, Salmond GP, Martinez-Salas E & Vincente M (1979) Role of the ftsA gene product in control of Escherichia coli cell division. *J. Bacteriol.* **140:** 388–394

Garner EC, Bernard R, Wang W, Zhuang X, Rudner DZ & Mitchison T (2011) Coupled, circumferential motions of the cell wall synthesis machinery and MreB filaments in B. subtilis. *Science* **333:** 222–225

Garner EC, Campbell CS & Mullins RD (2004) Dynamic instability in a DNA-segregating prokaryotic actin homolog. *Science* **306:** 1021–1025

Gayathri P, Fujii T, Moller-Jensen J, van den Ent F, Namba K & Lowe J (2012) A Bipolar Spindle of Antiparallel ParM Filaments Drives Bacterial Plasmid Segregation. *Science* **338:** 1334–1337

Gerdes K, Moller-Jensen J & Bugge Jensen R (2000) Plasmid and chromosome partitioning: surprises from phylogeny. *Mol. Microbiol.* **37:** 455–466

Hara F, Yamashiro K, Nemoto N, Ohta Y, Yokobori S-I, Yasunaga T, Hisanaga S-I & Yamagishi A (2007) An actin homolog of the archaeon Thermoplasma acidophilum that retains the ancient characteristics of eukaryotic actin. *J. Bacteriol.* **189:** 2039–2045

Jones LJ, Carballido-López R & Errington J (2001) Control of cell shape in bacteria: helical, actin-like filaments in Bacillus subtilis. *Cell* **104:** 913–922

Komeili A, Li Z, Newman DK & Jensen GJ (2006) Magnetosomes are cell membrane invaginations organized by the actin-like protein MamK. *Science* **311:** 242–245

Pettersen EF, Goddard TD, Huang CC, Couch GS, Greenblatt DM, Meng EC & Ferrin TE (2004) UCSF Chimera--a visualization system for exploratory research and analysis. *J Comput Chem* **25:** 1605–1612

Popp D, Narita A, Ghoshdastider U, Maeda K, Maéda Y, Oda T, Fujisawa T, Onishi H, Ito K & Robinson RC (2010a) Polymeric Structures and Dynamic Properties of the Bacterial Actin AlfA. *J. Mol. Biol.* **397:** 1031–1041

Popp D, Narita A, Oda T, Fujisawa T, Matsuo H, Nitanai Y, Iwasa M, Maeda K, Onishi H & Maéda Y (2008) Molecular structure of the ParM polymer and the mechanism leading to its nucleotide-driven dynamic instability. *EMBO J* **27:** 570–579

Popp D, Xu W, Narita A, Brzoska AJ, Skurray RA, Firth N, Ghoshdastider U, Goshdastider U, Maéda Y, Robinson RC & Schumacher MA (2010b) Structure and filament dynamics of the pSK41 actin-like ParM protein: implications for plasmid DNA segregation. *J. Biol. Chem.* **285:** 10130–10140

Porta JC & Borgstahl GEO (2012) Structural basis for profilin-mediated actin nucleotide exchange. *J. Mol. Biol.* **418:** 103–116

Terwilliger TC, Dimaio F, Read RJ, Baker D, Bunkóczi G, Adams PD, Grosse-Kunstleve RW,

    Afonine PV & Echols N (2012) phenix.mr_rosetta: molecular replacement and model

    rebuilding with Phenix and Rosetta. *J. Struct. Funct. Genomics* **13:** 81–90

van Teeffelen S, Wang S, Furchtgott L, Huang KC, Wingreen NS, Shaevitz JW & Gitai Z (2011)

    The bacterial actin MreB rotates, and rotation depends on cell-wall assembly.

    Proceedings of the ...

FIGURE LEGENDS:

Figure 1: Native Alp7A polymerizes into dynamic sheet-like bundles in the presence of ATP or GTP. (A) Polymerization of 17.5 μM Alp7A in the presence of 5mM ATP or GTP visualized by right angle light scattering. (B) Normalized maximum intensities of 25μM Alp7A in increasing ATP (open squares) and GTP (closed squares) concentrations. Alp7A has an apparent millimolar affinity for ATP and GTP. (C) 15uM Alp7A polymerized in ATP. (D) 15uM Alp7A polymerized in GTP.

Figure 2: The Structure of Alp7A as compared to homologs. (A) Comparison of ADP-Actin, (pdb 1J6Z, left), ADP-Alp7A (pdb 5EC0, center) and ADP-ParM from the R1 plasmid (pdb 1MWM, right). (C) Structure of Alp7A bound to ADP at 2.3 Angstroms with helices labeled. (D) Zoom of the nucleotide binding pocket with the electron density map. (E) Sequence alignment showing conserved residues involved in identifying Alp7A are the residues responsible for coordinating and hydrolyzing ATP. These residues define the Actin-Hsp70 super family of proteins.

Figure 3: Conserved and novel coordination of an unusual nucleotide conformation.
(A) Top view of the nucleotide showing conserved residues and bizarre nucleotide conformation of Alp7A: Actin (left), Alp7A (center) and ParM (right). (B) A comparison of the confirmations of the adenine moiety for Actin (pdb 1J6Z, left), Alp7A (pdb 5EC0, center), and ParM (pdb 1MWM, right). The residues coordinating the base are not conserved.

27

Figure 4: Conformation of the nucleotide is highly irregular with respect to all known nucleotide-bound structures.

(A) The Alp7A nucleotide is highly contorted with respect to the ribose pucker (pseudorotation) and base/ribose dihedral angle, relative to other actins, and most nucleotide bound structures in the pdb database, demonstrating that this is likely a high strain—but plausible—conformation. Grey: All ATP structures, Green: All ADP structures, Yellow: all eukaryotic actin structures, Pink, all bacterial actin structures.

SUPPLEMENTAL FIGURE LEGENDS:

Table 1: Table of Crystallography data

Table 2: Table describing the relative openness of bacterial actin-like proteins.

Figure S1: Filament architecture of native Alp7A

(A)5 µM Alp7A (B) 10 µM Alp7A (C) 12.5 µM Alp7A (D) 15 µM Alp7a (E) 20 µM Alp7A. (F) 30 µM Alp7A (D-F) shows irregular spacing of ribbon twists. All panels in the presence of 3mM ATP/Mg^{++}. Scale bars are 100nm.

Figure S2: Comparison of Bacterial actin protofilaments

(A) Comparison of the filament architecture of Eukaryotic actin (pdb 3g37, left), ParM filament (right) and Alp7A protofilaments from the crystal lattice (center). (B) Comparison of the

antiparallel subclass of 2D averaged filaments from the negative stain data and a 30A projection

of four protofilaments within the crystal lattice. In only one orientation of the crystal lattice are

the monomers offset from one another between protofilaments as seen in the 2D averages. That

orientation is shown here.

Figure S3: Alp7A with a C-terminal truncation forms filaments that are indistinguishable

from those of wild-type. (A) Antiparallel association of adjacent Alp7A protofilaments within

the crystal lattice. (B) Zoom of the black square from (A) shows the interaction of the c-terminal

tail with the adjacent monomer. (C) A titration of Alp7A 1-383 polymerized in 3mM ATP/Mg.

Maximum light scattering intensities are plotted as a function of Alp7A 1-383; the critical

concentration of Alp7A 1-383 is 12.5 +/- 0.8 μM.(d) 20uM Alp7a 1-383 in the absence of Alp7R.

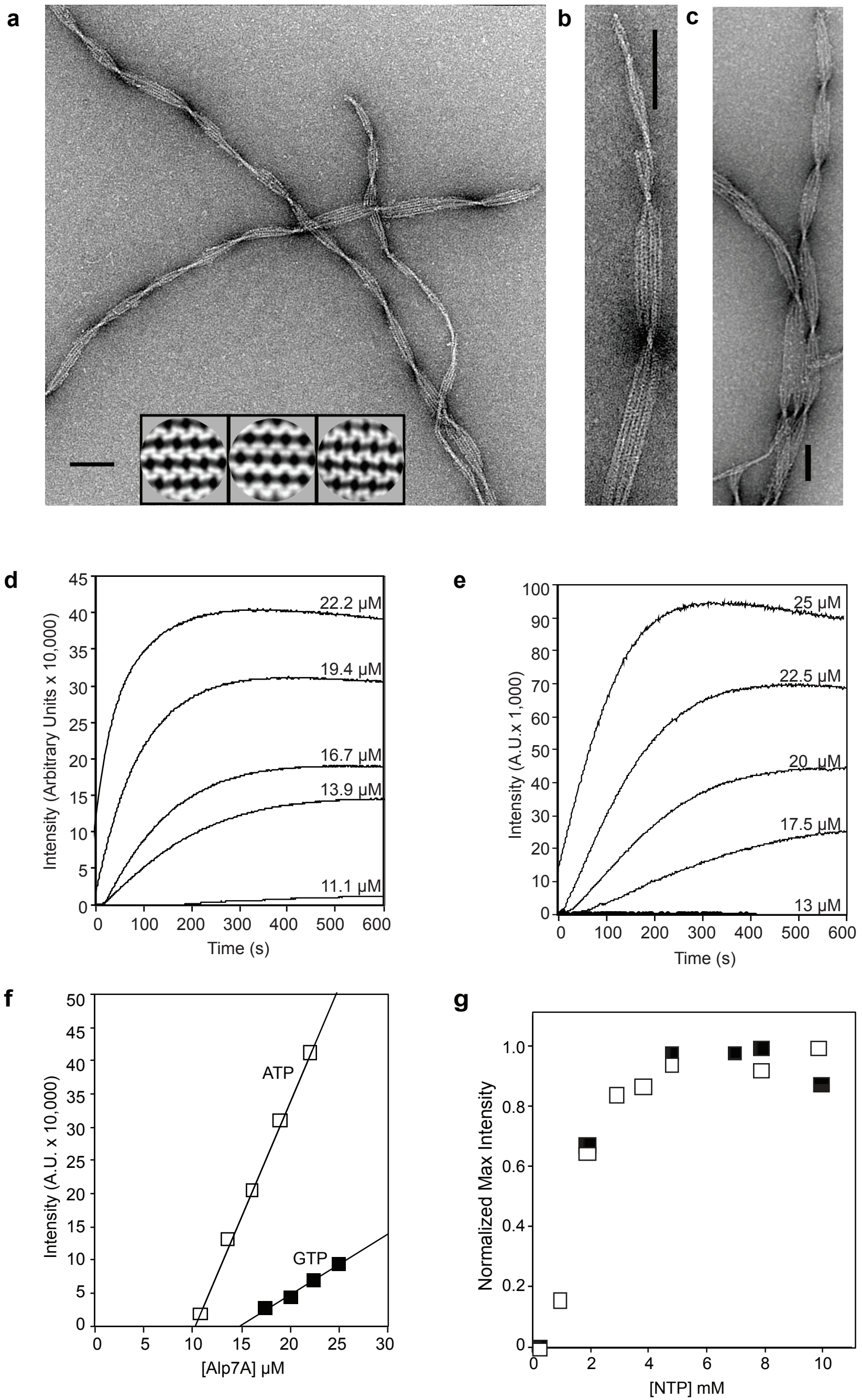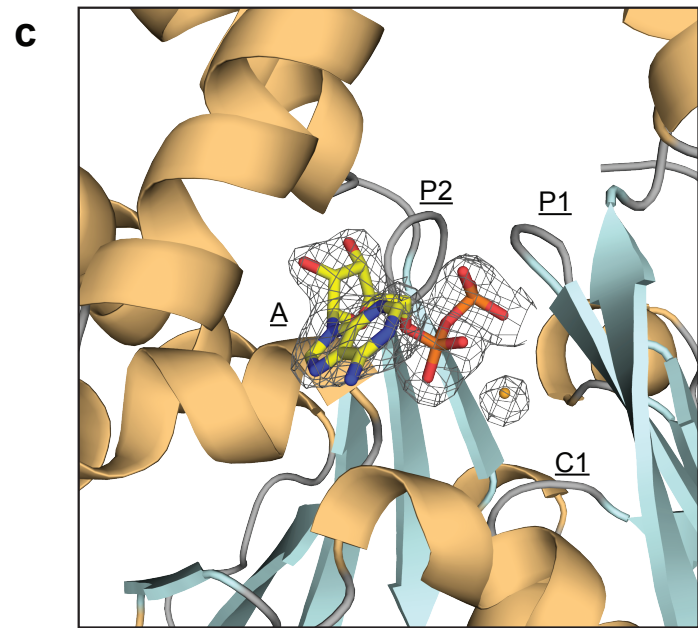Figure 1: Native Alp7A polymerizes into dynamic sheet-like bundles in the presence of ATP or GTP.

Figure 2: Comparison of Alp7A to other Actins

a

Actin | Alp7A | ParM

(Panel a labels: IV/IIB, II/IB, I/IA, III/IIA; IIB, IB, IA, IIA)

b

α-1, α-2, α-3, α-4, α-5, α-6, α-7, α-8, α-9, α-10, α-11, α-12, α-13

c

P2, P1, A, C1
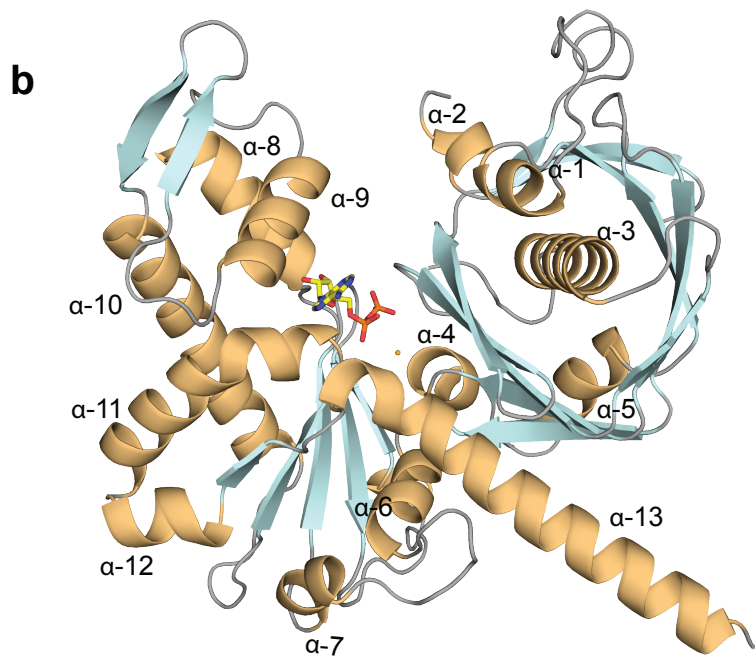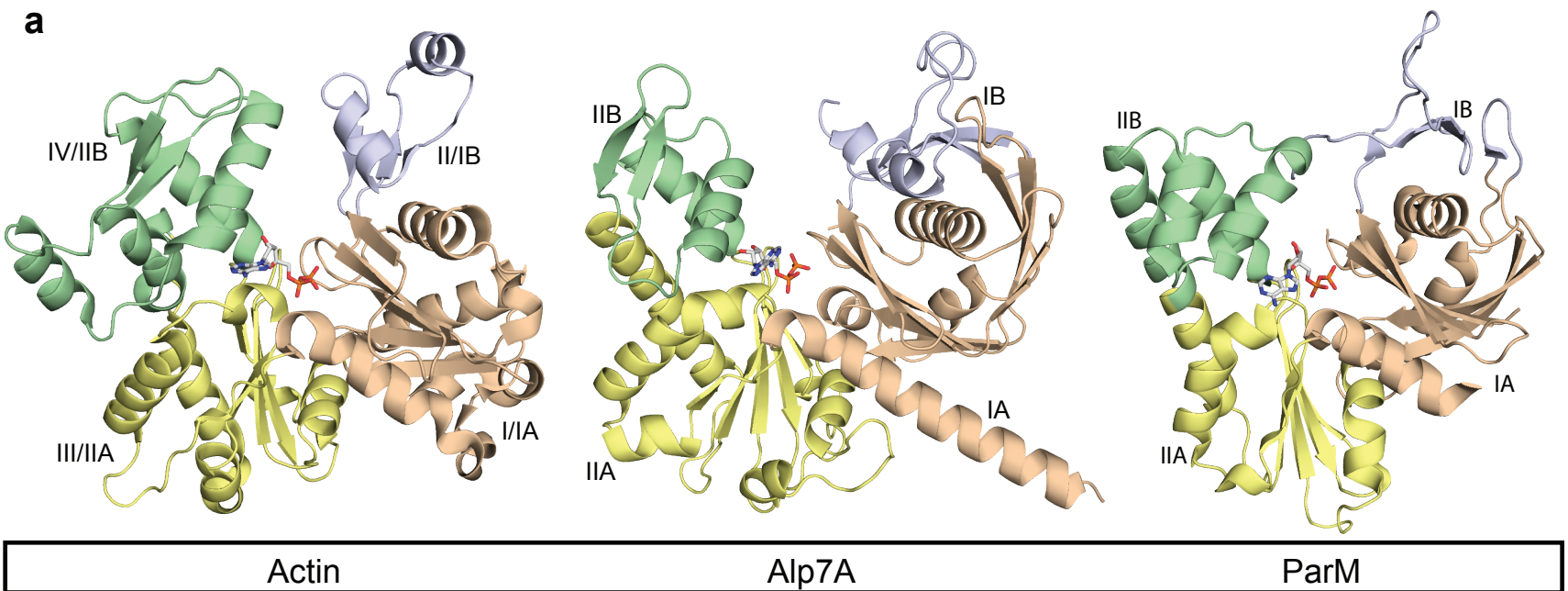
d

	PHOSPHATE 1	CONNECT 1	PHOSPHATE 2	ADENOSINE	CONNECT 2
ACTS_HUMAN	10 LVCDNGSGLV	136 VAIQAVLS	153 IVLDSGDGVTH	297 ANNVMSGGTTMYPG	339 YSVWIGGSILASL
MREB_ECOLI	13 LSIDLGTANT	140 LIEEPMAA	162 MVVDIGGGTTE	289 RGMVLTGGGALLRN	322 LTCVARGGGKALE
MREB_BACSU	5 GARDLGIDLG	133 PIEEPFAA	155 MVVDIGGGTTE	282 RGIVLTGGGALLRN	315 LDCVAIGTGKALE
AlfA/E9RJG4_BACNA	5 TVIDIGNFST	148 MAAEGLGA	165 VIVDAGSKTLN	219 YPIVCTGGKAEEMK	255 YYVNSVGLLLKYG
PARM_ECOLX	3 VFIDDGSTNI	145 VMPESIPA	167 LIIDLGGTTLD	274 THVMVIGGGAELIC	308 QYDLVNGMYLIGN
FTSA_BACSU	8 VSLDIGTSNT	183 ICLQPLAA	205 ALIDIGGGSTT	320 GGFVLTGGQAAMPG	360 QYMTGVGLIQFAC
MamK/Q6NE59_9PROT	27 LGIDLGTSHT	153 VVSEPFMV	171 IIVDLGAGTTD	295 QNIVFAGGGSRIRG	332 TFDGCRGALRLAE
Alp7A/E9RJ95_BACNA	6 MNVDFGNSMY	177 CRIESEVA	209 VFCDLGGGTDD	322 YKYLYFGGVGEVLE	363 RLLNLYGLEVLSR

Figure 3: Conserved and novel nucleotide coordination in Alp7A. A unique ATP

a

Actin   Alp7A   ParM

b
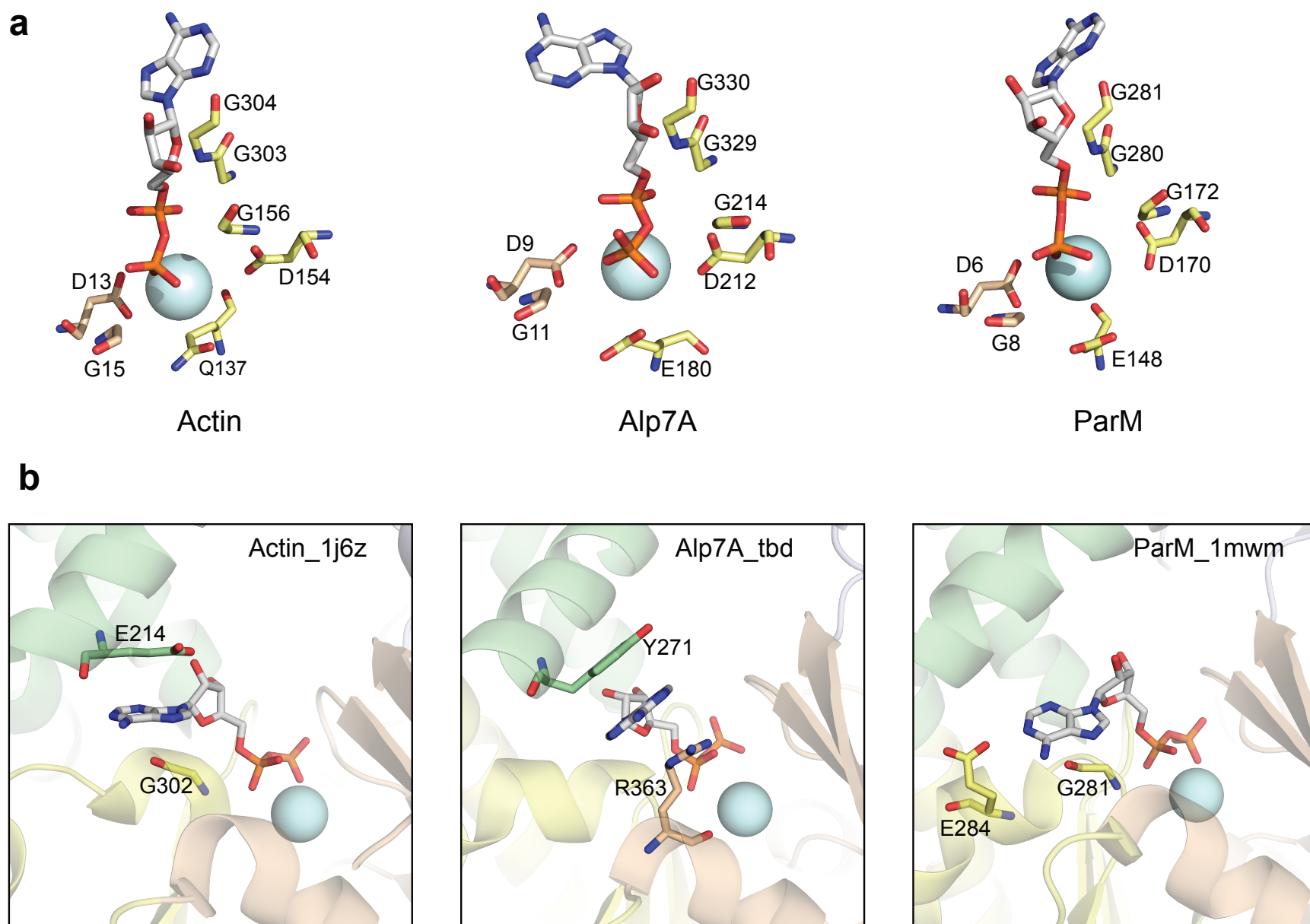
Figure 4: Conformation of the nucleotide is highly irregular with respect to actins, and all nucleotide bound structures.
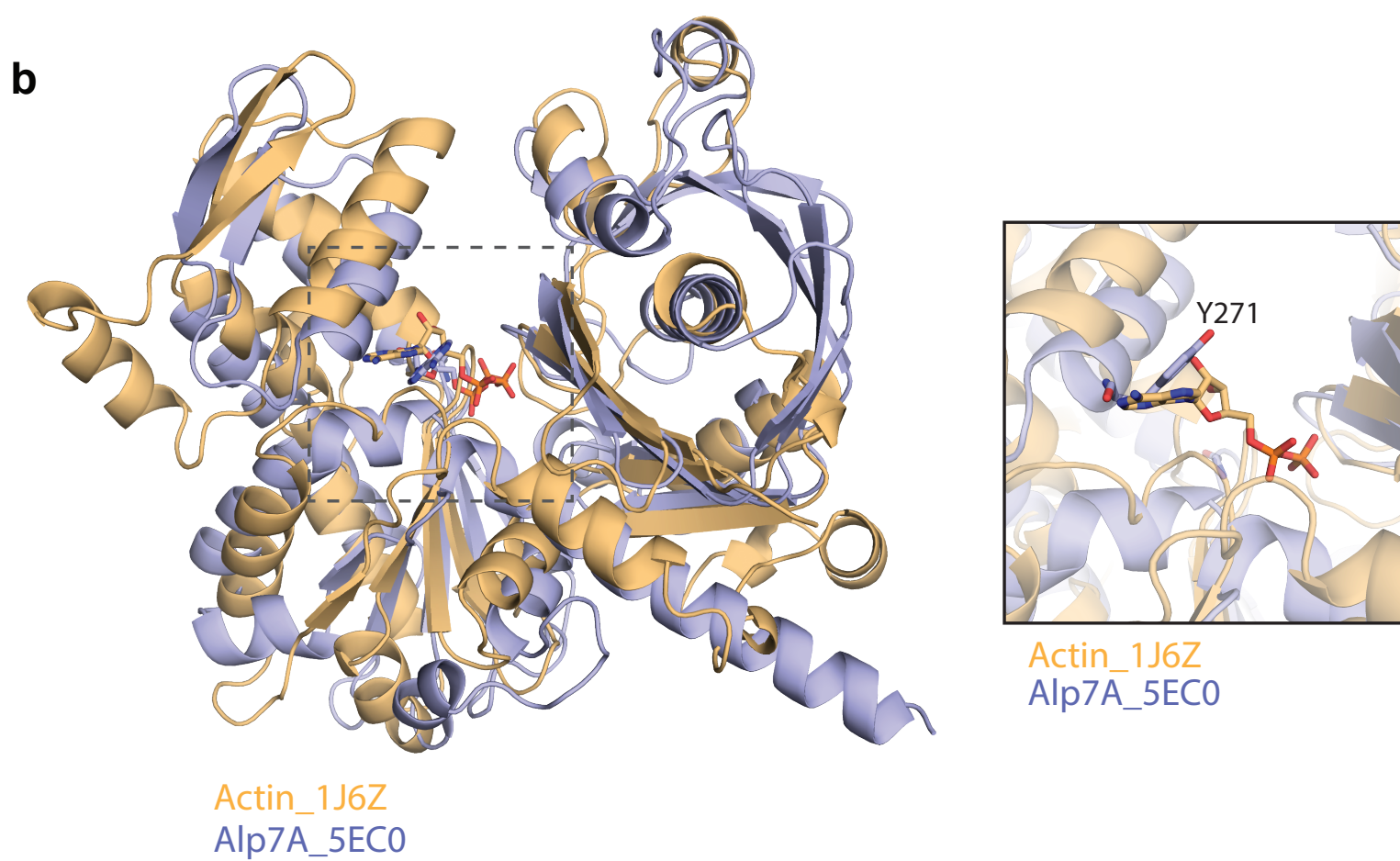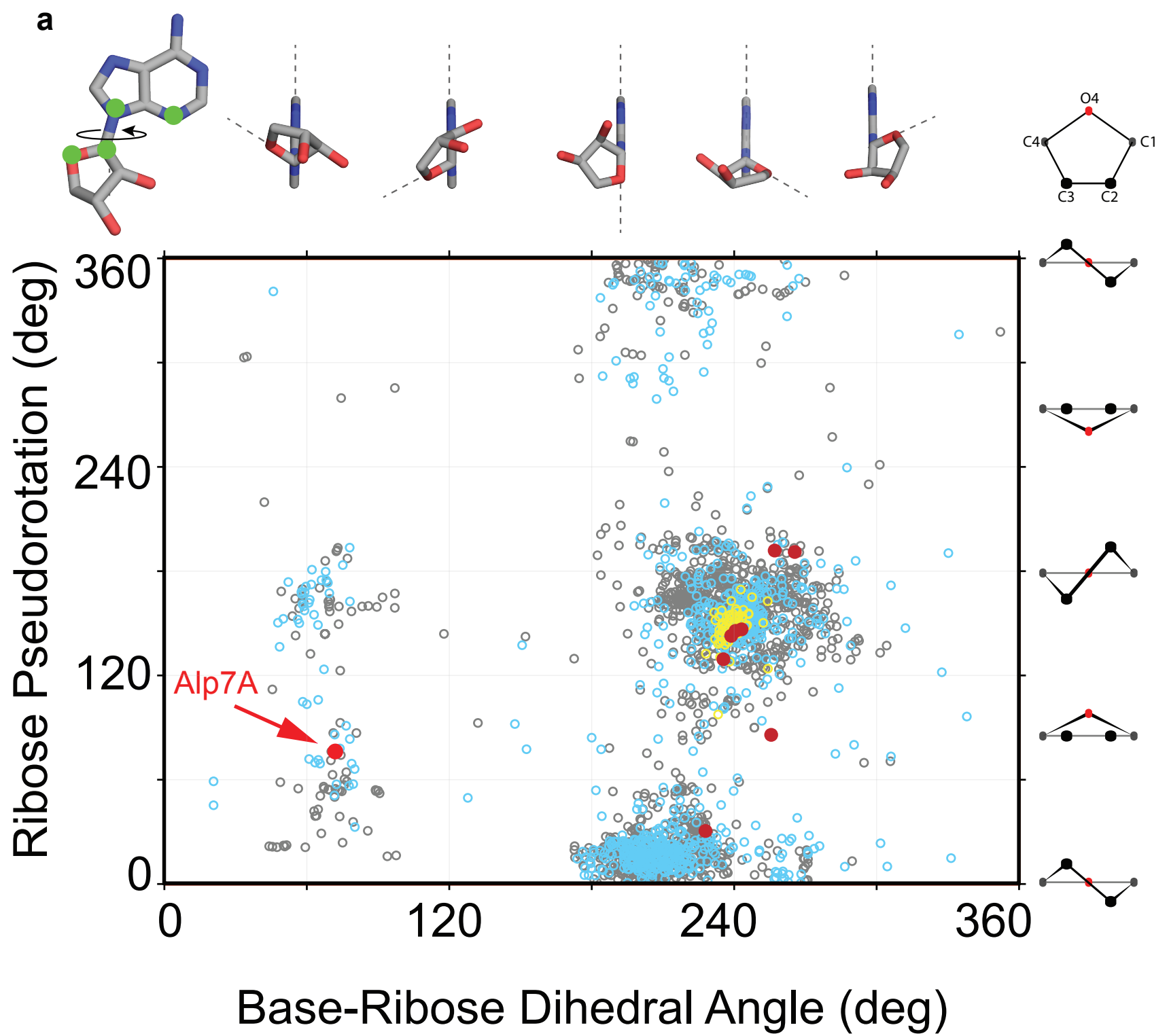
Table 1: Table of Crystallography data

Data Statistics	
Space group	$P2_12_12_1$
Unit cell dimensions (Å)	a=50.865, b=76.153, c=112.323 $\alpha=\beta=\gamma=90$
I/σ(I)	9.5 (1.25)
Completeness (%)	99.3 (95.2)
R_{sym} (%)	12.4
n_{refl}	22663
Structure Refinement	
Resolution range (Å)	39.6 − 2.2
R (%)	16.9 (24.8)
R_{fee} (%)	22.8 (30.1)
Protein residues	379
Water	148
ADP	1
Mg^{2+}	1
Average isotropic B-factors	
Protein atoms ($Å^2$)	45.5
Side-chain atoms ($Å^2$)	36.58
Solvent atoms ($Å^2$)	41.5
GDP ($Å^2$)	48.8
RMS Bonds (Å)	0.008
RMS Angles (°)	1.15
Ramachandran favored (%)	97
Ramachandran outliers (%)	0

Table 2: Relative openness of Actins

PDB	Protein	Nucleotide	Residues	Distance (Å)	Organism
1j6z	Actin	ADP	S14->G158	5.5	*Oryctolagus cuniculus*
1atn		ATP	S14->G158	5.5	
tba	Alp7A	ADP	N12->G216	7	*Bacillus subtilis (natto)*
4bql	Crenactin	ADP	T20->G185	6.8	*Pyrobaculum calidifontis*
4cj7		ADP	T20->G185	6.4	
4a2a	FtsA:FtsZ	ATP	S17->N216	7, 6.9	*Thermotoga maritima*
4a2b		ATP-γ-S	S17->N216	7.1	
1e4g	FtsA	ATP	S17->N216	7.2	
1e4f		APO	S17->N216	6.9	
1jce	MreB	APO	T12->G157	5.5	
1jcf		APO	T12->G157	5.5	
1jcg		AMP-PNP	T12->G157	5.6	
4czl		ADP	T19->G166	5.7	*Caulobacter crescentus*
4czg		ADP	T19->G166	5.7	
4czh		ADP	T19->G166	5.7	
4czf		ADP	T19->G166	5.7	
1mwm	ParM_R1	ADP	S9->T174	8, 8	*Escherichia coli*
1mwk		APO	S9->T174	10.9, 10.6	
4a61		AMP-PNP	S9->T174	7.2	
4a62		AMP-PNP	S9->T174	6.5	
4a6j		AMP-PNP	S9->T174	6.6	
2zgy		GDP	S9->T174	8, 8	
2zgz		GMP_PNP	S9->T174	7.8	
3js6	Psk41_Alp32	APO	N13->G194	9.7	*Staphylococcus aureus*
2fsn	Ta0583	ADP	Y10->R180	7.1	*Thermoplasma acidophilum*
2fsj		APO	Y10->R180	8	

Figure S1: Filament architecture of native Alp7A
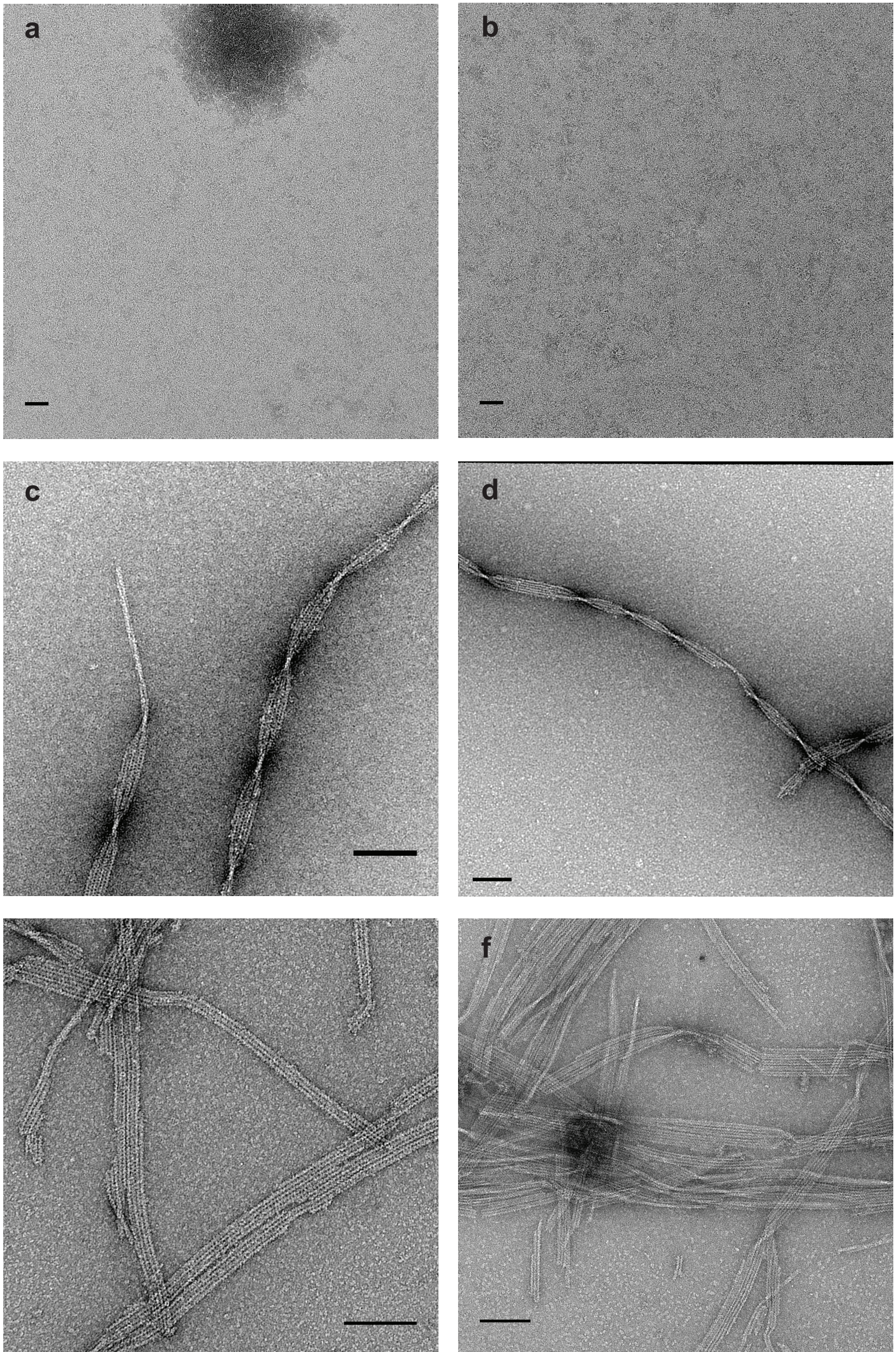
Figure S1: Comparison of Bacterial actin protofila-
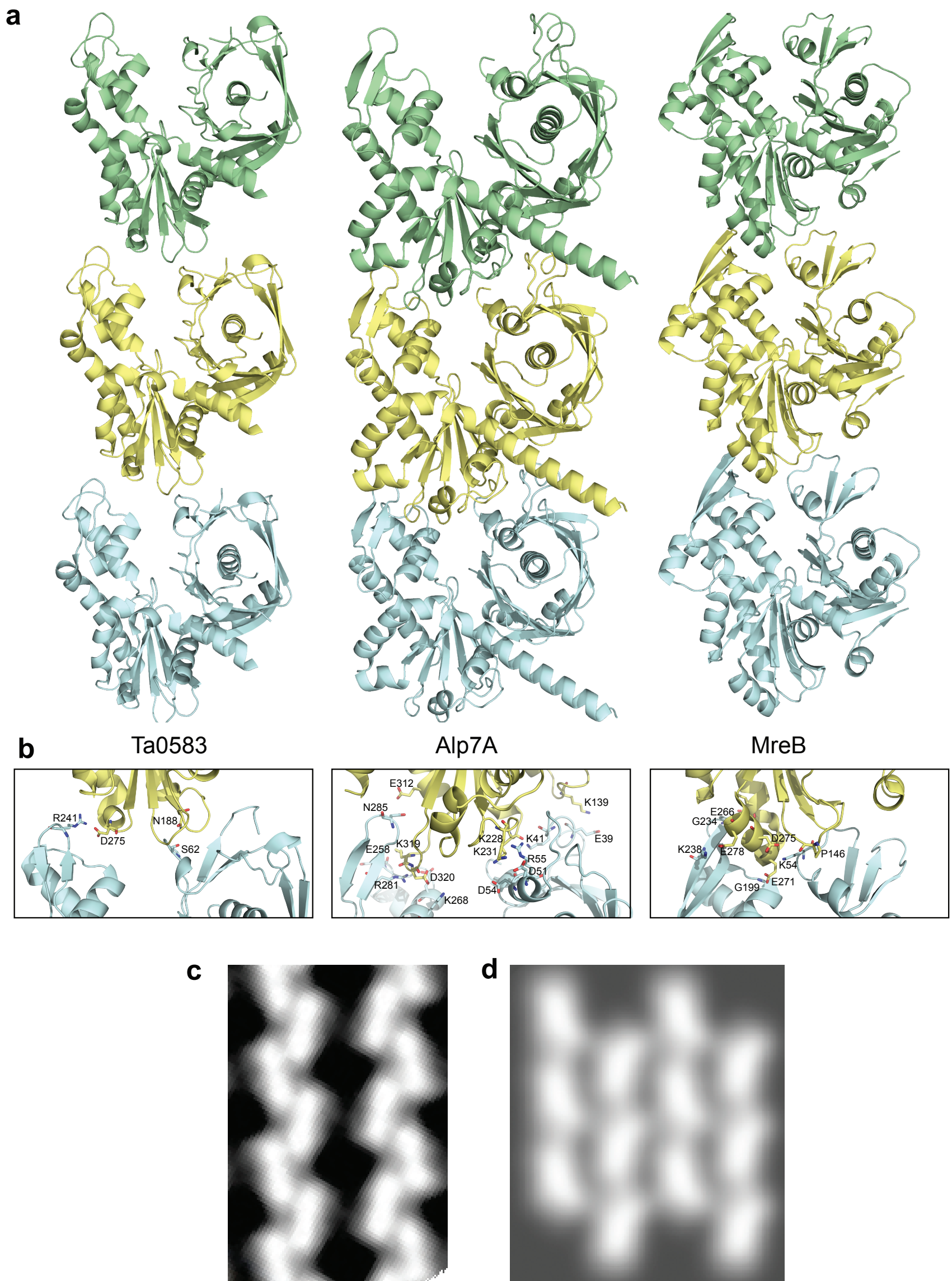
Figure S3: Alp7A with a C-terminal truncation forms filaments that are indistinguishable from those of wild-type.
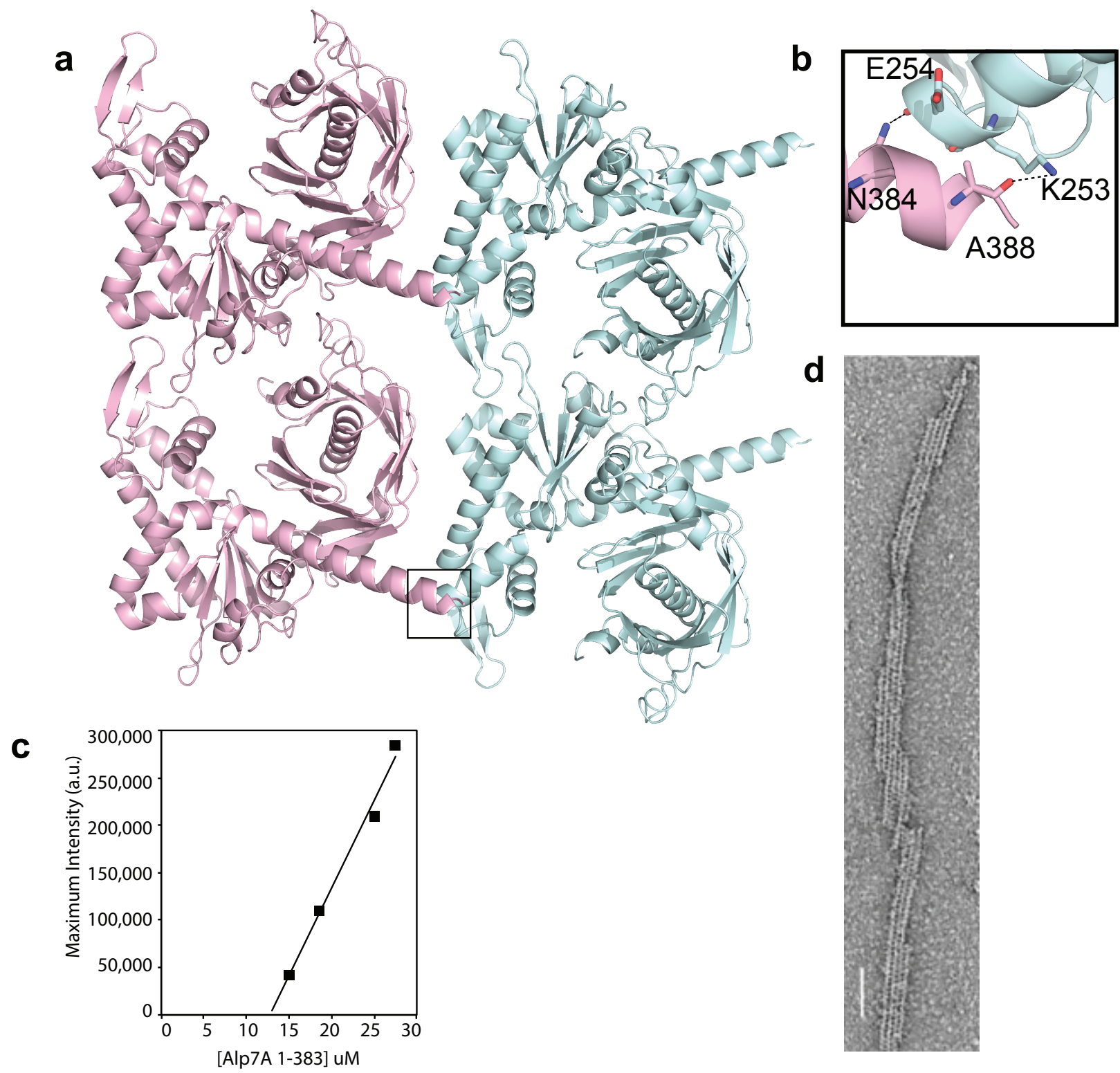
CHAPTER 3:

Alp7A reveals multiple mechanisms for creating and destroying dynamically unstable actin-like filaments.

Natalie Petek, James Kramer, Alan I. Derman, Jason A. Royal, James S. Fraser,

Frank DiMiao, David Baker, Joe Pogliano, David A. Agard and R. Dyche Mullins.

ABSTRACT:

Bacterial Actin-Like Proteins (ALPs) support many biologically, clinically, and commercially important processes. Previous work on plasmid DNA segregation revealed multiple mechanisms for creating, stabilizing, and destroying ALP filaments, some of which appear to be conserved and some of which do not. To better understand regulation of ALP assembly and function we studied the plasmid-segregating protein Alp7A, which revealed additional modes of regulation: single-step nucleation and nucleotide concentration-dependent destabilization. At low concentrations (<11 µM), Alp7A forms short-lived polymers. At higher concentrations these polymers are stabilized by forming mixed-polarity bundles. Surprisingly, the accessory factor Alp7R drives rapid, single-step nucleation of Alp7A filaments; stabilizes these new filaments; and prevents their bundling. These activities do not require plasmid DNA, which simply clusters Alp7R molecules.

INTRODUCTION:

Bacteria and Archaea express polymer-forming proteins related to eukaryotic cytoskeletal proteins, actin and tubulin. The Actin-Like Proteins (ALPs) found in bacteria participate in many fundamental biological processes including: cell wall assembly (Jones *et al*, 2001; Garner *et al*, 2011; Domínguez-Escobar *et al*, 2011; van Teeffelen *et al*, 2011), organelle positioning (Komeili *et al*, 2006), DNA segregation (Becker *et al*, 2006; Gerdes *et al*, 2000; Derman *et al*, 2009; Popp *et al*, 2010), and cytokinesis (Donachie *et al*, 1979). In addition, many low copy-number plasmids also employ ALPs to ensure their survival within bacterial populations by actively dispersing plasmid DNA so that it is more likely to be inherited by both daughter cells at the time of division. For example, Type-II plasmid-segregation operons encode both an actin-like protein and a DNA-protein complex that work together to promote plasmid inheritance. Polymerization of the actin-like protein generates force to move DNA through the cytoplasm, increasing the probability that both daughter cells will inherit at least one plasmid. Because of their simplicity —as well as their clinical significance— plasmid-segregating ALPs have become models for studying how polymer assembly drives biologically important processes.

To partition plasmids, a Type-II segregation system must do three things: (i) promote assembly of ALP filaments attached to plasmid DNA; (ii) convert ALP polymerization into plasmid movement; and (iii) couple the motion of two plasmids. Two distantly related ALPs —ParM (from plasmids found in Gram-negative rods) and AlfA (from *B. subtilis* plasmid pLS32)— have been studied in detail and their segregation systems have been reconstituted *in vitro* (Garner *et al*, 2007; Gayathri *et al*, 2012; Polka *et al*, 2014). Both ParM and AlfA couple the movement of

two plasmids by constructing spindles between them. Although their architectures differ, both spindles comprise mixed polarity filament bundles that elongate from their DNA-associated ends, pushing plasmids in opposite directions. Sustained polymerization of plasmid-associated filaments requires a concentration of monomeric ALP high enough for filament growth to outpace monomer dissociation. By analogy with eukaryotic actin filaments we define this concentration as the *critical concentration* for elongation or (for reasons described below) the *intrinsic* critical concentration. At steady-state, the monomer concentrations of both ParM and AlfA are maintained well above this intrinsic critical concentration by ATPase-driven mechanisms of filament destabilization (Garner *et al*, 2004; Polka *et al*, 2009). Importantly, this Atpase-driven destabilization —or *dynamic instability*— creates a second critical concentration, defined by the point at which the rate of filament formation balances the rate of catastrophic filament loss. We call this second balance point the *dynamic* critical concentration.

In the present study we describe the self-assembly of a plasmid-segregating actin-like protein, Alp7A, which shares less than 16% sequence identity with ParM and AlfA and whose *in vivo* behavior (Derman *et al*, 2009) poses significant challenges to the model of plasmid segregation derived from ParM and AlfA. I*n vivo* studies suggest that Alp7A, forms dynamically unstable filaments that interact with the Alp7R/C complex to create a DNA-segregating spindle, however unlike ParM and AlfA, Alp7A requires accessory factors for efficient and dynamic polymerization *in vivo* (Derman *et al*, 2009). The Alp7A gene forms part of the Alp7AR operon found in the pLS20 plasmid of *Bacillus subtilis* (natto). In addition to the actin-like protein Alp7A, this operon encodes a DNA binding protein, Alp7R, which binds to nine nearby DNA

sequence repeats (the Alp7C locus), to form a kinetochore-like complex (Derman *et al*, 2012). In the absence of Alp7R/C, polymer formation requires significant overexpression of Alp7A, and the polymers formed under these conditions do not appear to be dynamic or even filamentous (Derman *et al*, 2009). Surprisingly, these results suggest that, unlike previously described ALPs, the *critical concentration* for Alp7A polymerization is regulated by an accessory factor. Consistent with this idea, we find that the *dynamic* critical concentration of purified Alp7A measured *in vitro* is <11 µM: likely higher than the total cellular concentration of Alp7A. ATP hydrolysis assays and experiments with hydrolysis-dead mutants, however, reveal that Alp7A forms short-lived polymers well below 11 µM, and that the *intrinsic* critical concentration of Alp7A in ATP is ~20-fold lower (0.6 µM) than the *dynamic* critical concentration. By electron microscopy the dynamic critical concentration of purified Alp7A reflects the concentration at which ephemeral polymers survive long enough to laterally associate into more stable bundles (accompanying paper). The accessory factor Alp7R antagonizes the lateral self-association of Alp7A filaments while increasing the rate of filament nucleation. The net result of these changes is to prevent bundling-induced filament stabilization, but simultaneously lower the concentration of Alp7A at which filament creation balances filament destruction. These changes occur with no effect on the *intrinsic* critical concentration of polymer formation. This work reveals that the *dynamic* critical concentration of unstable actin-like filaments can be modulated by multiple mechanisms that have no effect on the underlying kinetics of polymer growth and shortening. Interestingly, the dynamic critical concentration of the three best-characterized, plasmid-segregating ALPs is each determined by the ability to laterally anneal, and may reflect a general theme for dynamically unstable polymers.

Surprisingly, our *in vitro* and *in vivo* experiments also reveal that Alp7R does not require DNA to stabilize Alp7A filaments. Soluble Alp7R molecules turn out to be sufficient to increase Alp7A nucleation *in vitro*, and DNA-independent clustering of Alp7R is sufficient to drive filament formation *in vivo*. Based on similarities in operon architecture, we suggest that this is a fundamental feature of all Type-II plasmid segregation systems.

RESULTS:

The interaction of Alp7A with Alp7R: effects on nucleation and architecture.

The best candidate for modulating the architecture and assembly dynamics of Alp7A polymers is

Alp7R, a DNA binding protein encoded in the same operon as Alp7A. Derman et al. (2009)

found that expression of Alp7R was required for efficient and dynamic Alp7A polymer formation

in vivo, we wanted to understand the nature of this regulation.

In the presence of ATP, the addition of purified, recombinant Alp7R to Alp7A disrupted bundles

at lower concentrations and converted the Alp7A ribbons (20:1 Alp7A:Alp7R) into well-

separated single filaments at at high Alp7R concentrations (2:1 Alp7A:Alp7R ratio) (Figure 1A).

The effect of Alp7R on the Alp7A bundles was concentration dependent and was unaffected by

the presence of the *alp7C* DNA.

In addition to inhibiting bundle formation, Alp7R also altered the kinetics of Alp7A assembly.

Addition of 0.5 µM Alp7R dramatically increased the rate at which 15µM Alp7A polymerized

(Figures 2A). Under these conditions the polymer reaches steady state in under 40 seconds,

compared to 500 seconds required for Alp7A alone. A kinetic analysis of Alp7A polymerization,

based on the work of Nishida and Sakai (Nishida & Sakai, 1983), indicates that the mechanism

of Alp7A nucleation (Figure 2A-B) changes from a four-step process in the absence of Alp7R to

a one-step process in the presence of Alp7R. Surprisingly, this effect does not require the

presence of DNA. Finally, we found that adding 500nM Alp7R to polymerization reactions

decreases the apparent critical concentration of Alp7A polymerization from 10.3 µM to

approximately 5.5 µM (Figure 2C-D). The affect of Alp7R on the critical concentration of

Alp7A is concentration dependent (Figure 2E); increasing the concentration of Alp7R further depresses the critical concentration of Alp7A.

Alp7R does not require DNA to nucleate filaments *in vivo*.

We next tested whether Alp7R can promote formation of Alp7A filaments *in vivo*, independent of its interaction with DNA. In addition to specific binding sites within *alp7C,* Alp7R also binds weakly to non-specific DNA. When expressed by itself, Alp7R-GFP localizes to the chromosome, lighting it up similar to DAPI-staining (Figure 3A). To prevent Alp7R from interacting non-specifically with chromosomal DNA, we tethered the protein to the cell envelope by fusing the *alp7R* gene to the *divIVA* gene, which encodes a cell division protein that is assembled into ring-shaped structures at the cell poles and septa (Eswaramoorthy *et al*, 2011). To gauge the effectiveness of this strategy, we first expressed a *divIVA*-a*lp7R-gfp* gene fusion that localized to polar and septal rings, a pattern characteristic of DivIVA localization. We observed no evidence of interaction with chromosomal DNA. From this experiment, we conclude that fusing Alp7R to the C-terminus of DivIVA does not interfere with DivIVA assembly, leaving it competent to control the localization of the fusion protein. We next expressed *divIVA-alp7R* together with *alp7A-gfp.* In this case we observed Alp7A-GFP localize to septal and polar rings and to form dynamic filaments that frequently emanate from these static rings (Fig 3A; Supp Movie 1). This observation strongly suggests that Alp7R does not need to bind DNA to nucleate dynamic Alp7A filaments *in vivo*.

The DNA-binding domain of Alp7R remained intact in the DivIVA-Alp7R fusion, so to more completely rule out a specific requirement for DNA binding, we constructed a variant fusion protein with a disrupted DNA-binding domain. The structure of Alp7R has not been solved, but the resemblance of its amino-terminal region to DNA-binding proteins of the RHH2 family together with the domain organization of similar proteins, such as ParR, suggested that the DNA-binding domain of Alp7R is at its amino terminus. We therefore removed the first 36 codons from *alp7R* in both the *divIVA-alp7R* and *divIVA-alp7R-gfp* contexts, to abolish DNA binding. Expression of *alp7RΔ36-gfp* failed to highlight the chromosome and distributed uniformly throughout the cytoplasm (Figure 3F). The *divIVA-alpRΔ36-gfp* fusion protein produced DivIVA-like polar and septal rings (Figure 3G), and expression of *divIVA-alpRΔ36* together with *alp7A-gfp* gave rise to the profile of the original *divIVA-alp7R* fusion, with dynamic filaments emanating from septal and polar rings (FIgure 3G, 3H). In this case though, filaments formed with no possibility of DNA binding, consistent with our biophysical finding that Alp7R could nucleate Alp7A filament formation independently of DNA *in vitro*.

ATP hydrolysis and Alp7A polymer assembly.

When we measured the rate of ATP hydrolysis, we found that purified Alp7A hydrolyzes ATP at a concentration-dependent rate, even at Alp7A concentrations below the apparent critical concentration of 10.3 µM (Figure 4A). This result suggests that Alp7R polymers form at these low concentrations but are too short-lived to be detected by co-pelleting or light scattering. Interestingly, addition of Alp7R decreases the steady state rate of ATP hydrolysis by Alp7A

47

(Figure 4C), suggesting that the decrease in apparent critical concentration caused by addition of Alp7R is due, at least in part, to stabilization of these ephemeral, spontaneously formed Alp7A filaments.

To better understand the role of ATP hydrolysis in the assembly and disassembly of Alp7A polymers, we constructed a hydrolysis-defective mutant of Alp7A. From our crystal structure, we identified a residue in the nucleotide binding pocket of Alp7A (E180) analogous to residues in ParM (E148) and actin (Q137) required for ATP hydrolysis (Garner *et al*, 2004; Vorobiev *et al*, 2003) and mutated it to an alanine (Alp7A-E180A). Consistent with a role for ATP hydrolysis in filament turnover, we found that Alp7A-E180A forms stable filaments with an apparent critical concentration much lower (0.6 ± 0.4 µM) than that of wildtype Alp7A (Figure 5A). This critical concentration matches the concentration above which we observe phosphate release, demonstrating that Alp7A forms filaments between 1-10uM which are rapidly disassembled due to hydrolysis. Interestingly, addition of Alp7R to the E180A mutant does not significantly decrease the apparent critical concentration of the mutant (Figure 5A). We propose therefore that this represents the <u>intrinsic</u> critical concentration of Alp7A filaments determined by the rate of elongation and shortening. This parameter is analogous to the ATP critical concentration of eukaryotic actin.

The hydrolysis-defective mutant also forms bundles, which are not disrupted by addition of Alp7R (Figure 5B), suggesting that the ability for Alp7R to disrupt bundle formation requires ATP hydrolysis and filament turnover. By contrast to the wildtype Alp7A, the E180A mutant is

stable in high salt. Attempts to disrupt the lateral filament associations with 1.5M NaCl instead resulted in a large fraction of the polymer being stabilized in small bundles (one to two double stranded filaments), in addition to the flattened sheet-like bundles (5C). This is likely because the high salt shields the bundles from the negatively charged surface of the grid, better preserving their three dimensional structure. This is apparent because filaments diluted with water formed only the flattened sheets, supporting the idea that Alp7A intrinsically forms bundles and the flattened ribbons we see in the electron microscope are an artifact of the charged grid.

DISCUSSION:

Our understanding of plasmid-segregating ALPs began with structure-function studies of the R1 *par* operon, and has now expanded to include comparisons of the molecular mechanisms employed by evolutionarily divergent systems (Polka *et al*, 2009; Rivera *et al*, 2011; Popp *et al*, 2010). The three best-studied ALPs —ParM, AlfA, and now Alp7A— share several properties that appear to define the minimal requirements for plasmid segregation: (i) dynamic instability; (ii) anti-parallel bundling; and (iii) plasmid-dependent filament stabilization. The very low sequence conservation among these ALPs and the significant divergence of other structural and biochemical features suggest that these shared properties are essential for plasmid segregation and have been maintained by positive selection. The present study reveals how ALP-based plasmid partitioning systems employ different mechanisms to maintain the rates of filament assembly, disassembly, and bundling in a regime that promotes formation of DNA-segregating spindles while causing minimal stress to the host cell.

Dynamic Instability

Although all of the well studied plasmid-segregating ALPs are dynamically unstable, their assembly properties exhibit remarkable diversity. The key to understanding this diversity lies in relationships between four fundamental parameters, the rates of filament: (i) elongation, (ii) shortening, (iii) nucleation, and (iv) catastrophe. Together, the rates at which **ATP-bound** filaments elongate and shorten define an intrinsic critical concentration, above which *individual filaments* grow steadily. Wildtype eukaryotic actin and mutant ALPs, defective in ATP hydrolysis, do not experience catastrophic depolymerization and so their assembly is dominated

by this intrinsic ATP critical concentration ((Garner *et al*, 2004); and this study). For wildtype ALPs the balance between rates of filament creation (nucleation) and loss (catastrophe) defines a second, dynamic critical concentration, above which the steady-state *number of filaments* is greater than zero. The dynamic critical concentrations of ParM, AlfA, and Alp7A are all higher than their intrinsic critical concentrations but these values can be shifted up or down by accessory factors or self-association. Interestingly, ParM has a high rate of spontaneous nucleation and a weak propensity to form bundles so its dynamic critical concentration is set directly by the rate of filament loss due to dynamic instability. In contrast, Alp7A has a much lower rate of spontaneous nucleation, which raises the concentration of Alp7A required for nucleation to balance catastrophe much higher than that of ParM. However, Alp7A has a strong tendency to form stable bundles, so its dynamic critical concentration is set by the rate at which newly formed filaments interact with each other. In other words, polymers appear when the average filament lifetime becomes comparable to the time required to form a stable bundle. The role of bundling in this monomer-to-polymer transition is apparent in the large number of steps required to form stable Alp7A bundles. Addition of the accessory factor, Alp7R, simultaneously increases the rate of Alp7A nucleation, stabilizes filaments against disassembly and disrupts bundling, making Alp7A filaments behave much more like ParM filaments. This result suggests that, while anti-parallel bundling is important for making a bipolar spindle (Gayathri *et al*, 2012; Polka *et al*, 2014), the stability of these bundles must be maintained within a window that is neither too high nor too low for proper spindle assembly and function.

DNA-independent effects of Alp7R on Alp7A polymerization

One surprising result of our work is that the accessory factor, Alp7R, does not require DNA for its effects on Alp7A filament assembly. This is surprising because the DNA binding component of a Type II plasmid segregation system must somehow couple actin-like filament assembly to the movement of DNA. Our *in vitro* and *in vivo* results both argue the *alp7C* locus performs this coupling function by simply clustering multiple Alp7R molecules on a small DNA locus. While soluble Alp7R induces rapid Alp7A nucleation throughout the cytoplasm, the Alp7R cluster at the segrosome provides a high-valency site of filament binding and stabilization. Therefore, despite significant differences in underlying assembly dynamics, both Alp7A and ParM filaments create DNA-segregating spindles with the same combination of fast, spatially distributed nucleation; localized filament stabilization; and weak anti-parallel bundling. Our results reveal that, while DNA segregation constrains parameters governing assembly of ALP-based spindles, the parameters themselves (e.g. rate of nucleation and strength of anti-parallel bundling) can either be intrinsic to the ALP or can be set by accessory factors.

Kinetic analysis reveals that Alp7R promotes single-step initiation of Alp7A polymers. In the simplest model for nucleation, Alp7R, which binds Alp7A monomers and forms dimers {Derman:2012ko, and this study}, brings two Alp7A protomers into contact in an orientation the mimics the end of a growing filament.

METHODS:

Expression and Purification of Alp7A

Alp7A was codon optimized (Mr. Gene) and cloned into the pet28a vector using the NcoI and HindIII restriction sites. Alp7A in Pet28 is freshly transformed for each purification into C43 cells and grown in TPM media at 37°C to an OD of 0.4-0.6, then shifted to 18°. Once temperature is achieved, cultures are induced overnight with 0.2mM IPTG. Cultures are pelleted, then washed with 1x PBS. Washed pellets are flash frozen in liquid nitrogen and stored at -80°C.

To purify native Alp7A, three liters of expression culture are resuspended in Lysis buffer (25mM Tris pH 7.6, 100 mM KCl, 1mM EDTA, 1mM DTT, PMSF). Cells are dounce homogenized pri or to lysis by 3x passes through an Emulsiflex-C3 (Avestin). The lysate is cleared with a high-speed spin (60 min at 170,000×g, 4°C) to remove cellular debris and insoluble protein. Ammonium sulfate is added slowly to the cleared lysate to 50% solubility, lysate is stirred at 4°C for one hour after all ammonium sulfate has been added. The precipitate is removed by centrifugation at 170,000xg for 30 minutes, 4°C. Alp7A is in the soluble fraction; the supernatant is transferred to a clean ultracentrifuge tube and brought to room temperature using an ambient water bath. 5 mM ATP/6 mM $MgCl_2$ are then added to induce polymerization. After a 15 minute incubation, the polymer is pelleted by high speed centrifugation (20 min at 170,000×g, 25°C) and then resuspended in 1/10 volume of cold depolymerization buffer (25mM Tris pH 7.6, 200mM KCl, 6mM EDTA, 1mM DTT). The resuspended protein is dialyzed overnight to remove residual ATP and ensure complete depolymerization. Alp7A is gel filtered on Superdex S-200 resin into polymerization buffer (25 mM Tris pH 7.6, 100 mM KCl, 1 mM $MgCl_2$, 1mM

DTT); the purest protein fractions are pooled and dialyzed into storage buffer (polymerization buffer + 20% glycerol). Aliquots are snap frozen in liquid nitrogen and stored at -80°C. Protein is quantified by the Alp7A extinction coefficient $34,965 M^{-1}cm^{-1}$.

Expression and Purification of Alp7R:

 A pE-SUMOstar vector (LifeSensors) containing the Alp7R insert was transformed into BL21 cells. Cultures are grown in LB media to an OD of 0.4-0.6, then induced for 4 hours with 0.750 mM IPTG. Cultures are pelleted and washed with 1x PBS. Washed pellets are flash frozen in liquid nitrogen then stored at -80°C.

To purify 6x-his-SUMO-Alp7R, cells from two liters of culture were resuspended in lysis buffer (50mM HEPES pH 8.0, 400mM NaCl, 1mM BME + cOmplete EDTA free protease inhibitor-Roche). Cells were dounce homogenized prior to lysis by 3x passages through an Emulsiflex-C3 (Avestin). The lysate is cleared with a high-speed spin (60 min at 170,000×g, 4°C) to remove cellular debris and insoluble protein. Protein is bound to a 5mL HiTrap Chelating HP column precharged with $CoCl_2$, washed with lysis buffer, then eluted with 500mM Imidazole. The most concentrated fractions are pooled, then incubated for 30 min at room temperature with SUMO Protease I (90+% cleaved after this step). This is then dialyzed over night in 50mM HEPES pH 8.0, 400mM NaCl, 1mM BME. The cleaved tag and uncleaved protein are then removed by running the protein over a 1ml HiTrap Chelating HP column. The eluate is gel filtered on Superdex S-200 resin. Peak fractions are pooled and dialyzed into 25mM HEPES, 400mM NaCl, 1mM DTT, 20% glycerol. Aliquots are snap frozen in liquid nitrogen and stored at -80°C. Protein

is quantified by Sypro Ruby (S-12000. Molecular Probes™) staining as Alp7R contains no endogenous tryptophans.

Amplification of Alp7C

Alp7C is amplified by PCR of the Alp7C region from the mini-plS20 plasmid (courtesy of Joe Pogliano) using the methods described in Derman et. al., 2012.

Negative Stain Electron Microscopy

Samples are prepared by applying 4ul of polymerization mix to 200mesh Formvar carbon film coated (Electron Microscopy Sciences-FCF200-Cu) glow discharged grids and incubating for 30 seconds. Grids are washed 3x in buffer, blotting between washes. Grids are stained 3x with 0.75% uranyl formate, blotting between applications. The third stain step is done for 30 sec. Micrographs were taken with a Technai T12 microscope using an acceleration voltage of 120 kV and a magnification of x27,000 or x48,000. Images were recorded with a Gatan 4k x 4k charge-coupled device camera.

Right Angle Light Scattering

Light scattering experiments were performed using an ISS K2 fluorimeter at a wavelength of 320nm. Polymerization of Alp7A was induced by hand mixing or use of a SFA-20 rapid mixer (Hi-Tech) coupled to the fluorimeter. For each condition four to five traces were background subtracted and averaged. The critical concentration, or steady state monomer concentration, of

Alp7A was determined by plotting the maximum light scattering intensity of averaged traces versus the concentration of Alp7A. The x-intercept of this line is the value for the critical concentration.

Plasmids and plasmid constructions. The plasmids used in this study are listed in Supplementary Table 1. The construction of plasmid pAID3219 (pP*xyl*alp7R-gfp), where *gfp* encodes green fluorescent protein, was described previously (Derman *et al.*, 2012). Plasmid pAID3604 (pP*xyl*alp7RΔ36-gfp) was constructed by amplification of pAID3129 with oligonucleotide primers P1 and P2, restriction of the amplicon with AvrII and SphI, and ligation to pAID3129 restricted with AvrII and SphI. Plasmids and ligation mixtures were introduced into *E. coli* DH5α by electroporation or by transformation of chemically competent cells.

Bacterial strains, strain construction, and growth of bacteria. The strains used in this study are listed in Supplementary Table 1. Strain JP3348 (PY79 *amyE*::P*hyspank*divIVA-alp7R-gfp) was constructed by integration into the PY79 chromosome of a modified version of plasmid pDR197, a derivative of the *B. subtilis* integration vector pDR111[31] that contains a *divIVA-gfp* gene fusion under control of the *hyperspank* promoter (Ramamurthi and Losick. 2009). Plasmid pAID3129 was amplified with oligonucleotide primers P3 and P4, and the amplicon was cloned into the pCR2.1-TOPO vector (Life Technologies). The 429 bp segment containing the *alp7R* gene followed by sequence coding for the seven amino acid linker RPEDIH was excised with NheI and ligated to pDR197 restricted with NheI. The tripartate gene fusion on the resulting plasmid was then integrated into the PY79 chromosome at *amyE* by a double recombination event. The same strategy was used to construct strain JP3350 [PY79 *amyE*::P*hyspank*divIVA-alp7R*TAA*-gfp *thrC*::(P*xyl*alp7A-gfp)], except that primer P5, which preserves the *alp7R* stop

codon, was used in place of P2, and strain JP3161 [PY79 *thrC*::P*xyl*alp7A-gfp)] was used for integration. Strains JP3569 [PY79 *amyE*::(*lacI*+ P*hyspank*divIVA-alp7RΔ36-gfp spec)] and JP3568 [JP3161 *amyE*::(*lacI*+ P*hyspank*divIVA-alp7RΔ36*TAA*-gfp spec)] were constructed by integration into PY79 and JP3161 of versions of the integration plasmids in which the first 36 codons of *alp7R* had been deleted. The *alp7RΔ36* deletion in JP3569 was constructed by amplification of the P*hyspank*divIVA-alp7RΔ36-gfp integration plasmid with oligonucleotide primers P6 and P7, restriction of the amplicon with NheI and AatII, and ligation to pDR197 restricted with NheI and AatII. The *alp7RΔ36*TAA deletion in JP3568 was constructed by oligo-directed deletion mutagenesis of the P*hyspank*divIVA-alp7RΔ36*TAA*-gfp integration plasmid with mutagenic oligonucleotide primers P8 and P9 as described (Derman *et al.*, 2012). These plasmids were then integrated into PY79 or JP3161 at *amyE*. The orientation of each *alp7R* insertion was evaluated by restriction endonuclease digestion and the sequences verified by DNA sequencing. Only background green fluorescence could be detected from control strains JP3349 [PY79 *amyE*::P*hyspank*divIVA-alp7R*TAA*-gfp] and JP3567 [PY79 *amyE*::P*hyspank*divIVA-alp7RΔ36*TAA*-gfp] at all induction levels surveyed, indicating that there was no read-though into *gfp* when the *alp7R* stop codon was present.

Media and antibiotic supplementation was as described (Derman *et al.*, 2012).

Microscopy. Agarose pads for microscopy were prepared and imaged as described (Derman et *al.*, 2012).

Oligonucleotide Primers

P1: 5'-gtactcctagggaggcacaatcaatttaggtgattagaaatgaaaagtaagggtacctttagagagtatgc-3'

P2: 5'-gtactgcatgcgacctcgtttccaccggaattag-3'

P3: 5'-ctgtagctagcatggggaaaaacaaaagaattccac-3'

P4: 5'-gtactgctagcatgtatatctccttccggccgaaaatcatagtcgtattcttcttcaatag-3'

P5: 5'-gtactgctagcatgtatatctccttccggccgttaaaaatcatagtcgtattcttcttcaatag-3'

P6: 5'-ctgtagctagcagtaagggtacctttagagag-3'

P7: 5'-catttatcagggttattgtctc-3'

P8: 5'-gaggaaaaggaagctagcagtaagggtacctttagagag-3'

P9: 5'-ctctctaaaggtacccttactgctagcttccttttcctc-3'

Phosphate Release Assays

Phosphate release assays were performed using the Enzcheck Phosphate Assay Kit (Invitrogen-E6646) and an Ultraspec 2100 Pro spectrophotometer (GE Healthcare Lifesciences). Both protein, and ATP/MgCl$_2$ mixtures were pre-incubated with the Enzcheck reagents to remove any contaminating phosphate that might convolute the experimental results.

REFERENCES:

Becker E, Herrera NC, Gunderson FQ, Derman AI, Dance AL, Sims J, Larsen RA & Pogliano J (2006) DNA segregation by the bacterial actin AlfA during Bacillus subtilis growth and development. *EMBO J* **25:** 5919–5931

Derman AI, Becker EC, Truong BD, Fujioka A, Tucey TM, Erb ML, Patterson PC & Pogliano J (2009) Phylogenetic analysis identifies many uncharacterized actin-like proteins (Alps) in bacteria: regulated polymerization, dynamic instability and treadmilling in Alp7A. *Mol. Microbiol.* **73:** 534–552

Derman AI, Nonejuie P, Michel BC, Truong BD, Fujioka A, Erb ML & Pogliano J (2012) Alp7R regulates expression of the actin-like protein Alp7A in Bacillus subtilis. *J. Bacteriol.* **194:** 2715–2724

Domínguez-Escobar J, Chastanet A, Crevenna AH, Fromion V, Wedlich-Söldner R & Carballido-López R (2011) Processive movement of MreB-associated cell wall biosynthetic complexes in bacteria. *Science* **333:** 225–228

Donachie WD, Begg KJ, Lutkenhaus JF, Salmond GP, Martinez-Salas E & Vincente M (1979) Role of the ftsA gene product in control of Escherichia coli cell division. *J. Bacteriol.* **140:** 388–394

Eswaramoorthy P, Erb ML, Gregory JA, Silverman J, Pogliano K, Pogliano J & Ramamurthi KS (2011) Cellular architecture mediates DivIVA ultrastructure and regulates min activity in Bacillus subtilis. *MBio* **2:**

Garner EC, Bernard R, Wang W, Zhuang X, Rudner DZ & Mitchison T (2011) Coupled, circumferential motions of the cell wall synthesis machinery and MreB filaments in B. subtilis. *Science* **333:** 222–225

Garner EC, Campbell CS & Mullins RD (2004) Dynamic instability in a DNA-segregating prokaryotic actin homolog. *Science* **306:** 1021–1025

Garner EC, Campbell CS, Weibel DB & Mullins RD (2007) Reconstitution of DNA segregation driven by assembly of a prokaryotic actin homolog. *Science* **315:** 1270–1274

Gayathri P, Fujii T, Moller-Jensen J, van den Ent F, Namba K & Lowe J (2012) A Bipolar Spindle of Antiparallel ParM Filaments Drives Bacterial Plasmid Segregation. *Science* **338:** 1334–1337

Gerdes K, Moller-Jensen J & Bugge Jensen R (2000) Plasmid and chromosome partitioning: surprises from phylogeny. *Mol. Microbiol.* **37:** 455–466

Jones LJ, Carballido-López R & Errington J (2001) Control of cell shape in bacteria: helical, actin-like filaments in Bacillus subtilis. *Cell* **104:** 913–922

Komeili A, Li Z, Newman DK & Jensen GJ (2006) Magnetosomes are cell membrane invaginations organized by the actin-like protein MamK. *Science* **311:** 242–245

Nishida E & Sakai H (1983) Kinetic analysis of actin polymerization. *J. Biochem.* **93:** 1011–1020

Polka JK, Kollman JM & Mullins RD (2014) Accessory factors promote AlfA-dependent plasmid segregation by regulating filament nucleation, disassembly, and bundling. *Proc. Natl. Acad. Sci. U.S.A.* **111:** 2176–2181

Polka JK, Kollman JM, Agard DA & Mullins RD (2009) The structure and assembly dynamics of plasmid actin AlfA imply a novel mechanism of DNA segregation. *J. Bacteriol.* **191:** 6219–6230

Popp D, Xu W, Narita A, Brzoska AJ, Skurray RA, Firth N, Ghoshdastider U, Goshdastider U, Maéda Y, Robinson RC & Schumacher MA (2010) Structure and filament dynamics of the pSK41 actin-like ParM protein: implications for plasmid DNA segregation. *J. Biol. Chem.* **285:** 10130–10140

Rivera CR, Kollman JM, Polka JK, Agard DA & Mullins RD (2011) Architecture and assembly of a divergent member of the ParM family of bacterial actin-like proteins. *J. Biol. Chem.* **286:** 14282–14290

van Teeffelen S, Wang S, Furchtgott L, Huang KC, Wingreen NS, Shaevitz JW & Gitai Z (2011) The bacterial actin MreB rotates, and rotation depends on cell-wall assembly. *Proceedings of the …*

Vorobiev S, Strokopytov B, Drubin DG, Frieden C, Ono S, Condeelis J, Rubenstein PA & Almo SC (2003) The structure of nonvertebrate actin: implications for the ATP hydrolytic mechanism. *Proc. Natl. Acad. Sci. U.S.A.* **100:** 5760–5765

FIGURE LEGENDS:

Figure 1: Alp7R disrupts bundling of Alp7A

(a) 20 µM Alp7A assembled in the presence of 0.5 µM (top), or 1.0 µM (middle) and 8 µM

Alp7A in the presence of 4 µM Alp7R (bottom).

Figure 2: Alp7R alters the polymerization kinetics and nucleation of Alp7A filaments

(b) A titration of Alp7A polymerized in the presence of 0.5 µM Alp7R. (c) The steady state

monomer concentration of Alp7A is depressed approximately two-fold in the presence of 0.5µM

Alp7R. Maximum intensity plots of a titration of Alp7A in the absence (open squares) and

presence (closed squares) of Alp7R. (d) Critical concentration of Alp7A in the presence of 0.1

µM Alp7R (black circles), 1.0 µM Alp7R (green squares), or 5.0 µM Alp7R (pink squares). (e)

Comparison of 15 µM ALp7A polymerized in the presence or absence of 0.5µM Alp7R. Inset

shows a zoom of the first 20 seconds of polymerization. (f) Analysis of nucleation mechanism as

described by Sakai et al. wherein the log of the maximum velocity is plotted versus the log of

protein concentration. Twice the slope of this line describes the number of kinetically resolvable

nucleation steps.

Figure 3: Alp7R nucleates filaments *in vivo* in the absence of DNA

(a)Alp7R-GFP nonspecifically coats DNA in the absence of the specific Alp7C DNA sequence.

The top panel shows membrane in red, middle is Alp7R-GFP, bottom shows DNA by DAPI

staining. (b) The DivIVA-Alp7R fusion correctly localizes to the cell pole as seen by: membrane

staining (top) overlay (middle) and DivIVA-Alp7R-GFP (bottom). (c) Alp7A-GFP is diffuse in

the absence of Alp7R: cell membranes (top), overlay (center), Alp7A-GFP (bottom). (d) Alp7A

forms filaments that nucleate from the cell pole in the presence of the DivIVA fusion protein. The

top panel shows cell membranes, the center shows the overlay, and the bottom panel shows

filaments of Alp7A-GFP nucleating from the cell pole. (e) A montage of two cells (dotted square

in d) over time shows Alp7A-GFP nucleating, elongating and undergoing catastrophic

disassembly (left cell). All scale bars: 1 μm.

Figure 4: Alp7A is highly dynamic and forms ephemeral filaments well below the dynamic

critical concentration in the absence of Alp7R

Alp7A bundles are highly dynamic. (a) Rapid disassembly of polymerized Alp7A at steady state.

At the red arrow 25uM Alp7A is diluted by addition of 3x polymerization buffer without ATP;

total concentration is 8.3 μM Alp7A. (b) Phosphate release rates plotted as a function of protein

concentration show that Alp7A is polymerizing below the apparent critical concentration (steady

state monomer concentration), ie. hydrolysis is occurring at 1μM and 5μM Alp7A (c) Single

phosphate release traces show differences in the steady state phosphate release rates when Alp7R

is present. Steady state phosphate release is slower in the presence of Alp7R.

Figure 5: Alp7R depresses the critical concentration of Alp7A by stabilizing highly

ephemeral filaments.

(a) The hydrolysis dead mutant Alp7A_E180A has a critical concentration of 0.6μM Alp7A

(open squares). This is not significantly reduced in the presence of Alp7R (closed squares). (b-d)

Alp7A_E180A sheets are not disrupted by addition of Alp7R suggesting that this process

requires filament turnover and/or nucleotide hydrolysis. At 1μM Alp7A-E180A the polymeric

structure is highly bundled (b). (c) In the presence of equimolar Alp7R, Alp7A-E180A still

forms bundles . (d) Addition of 1.5M NaCl does not disassociate bundles, but instead shields the

bundles from the highly charged grid, diminishing the occurance of flattened sheets . Bundles are

10-15nm in width, which are likely one to two-stranded bundle.

Figure 6: Models of nucleation. How nucleation/bundling unstable filaments differ from two-

stranded filaments. How does Alp7R nucleate filaments of Alp7A?

(a) Nucleation of a two-stranded filament. Three kinetically resolvable steps form a stable

nucleus(top). Nucleation of a nucleation/bundling unstable filament. The additional step of

lateral annealing is required to form a stable nucleus, resulting in four+ kinetically resolvable

steps for nucleation.

(b) Model for in-vitro nucleation of Alp7A by Alp7R. Dimers of Alp7R can bind to two Alp7A

monomers forming a "pre-nucleation" complex. Upon addition of ATP, only one step is required

to form a stable nucleus. Side binding of Alp7R to Alp7A filaments stabilizes filaments against

disassembly (top). In-vivo, Alp7R dimers are bound with high affinity to Alp7C or are tethered

to the pole by DivIVA. These dimers can interact with Alp7A monomers, increasing the local

concentration of Alp7A and additionally forming a "pre-nucleus."

Figure 1: Alp7R disrupts bundling of Alp7A
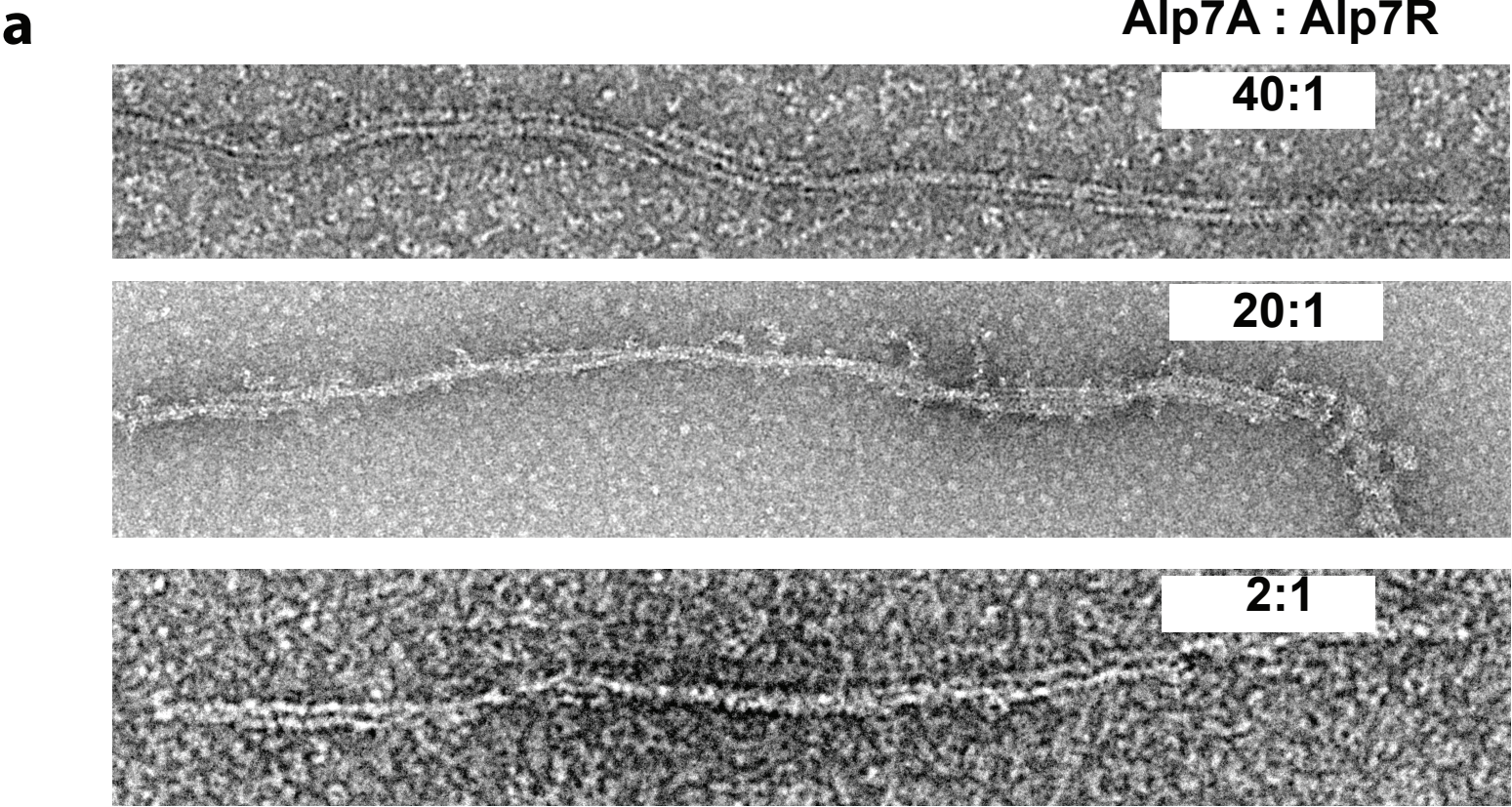
66

a

Alp7A : Alp7R

Figure 2: Alp7R alters the polymerization kinetics and nucleation of Alp7A filaments

Figure 3: Alp7R nucleates filaments in vivo in the absence of DNA

a Alp7R-GFP

b DivIVA-Alp7R-GFP

e
0
6
9
15
18
24
33
36
63

c Alp7A-GFP (no Alp7R)

d Alp7A-GFP (with DivIVA-Alp7R)

f Alp7R(37-135)-GFP

g Alp7A-GFP (with DivIVA-Alp7R(37-135))
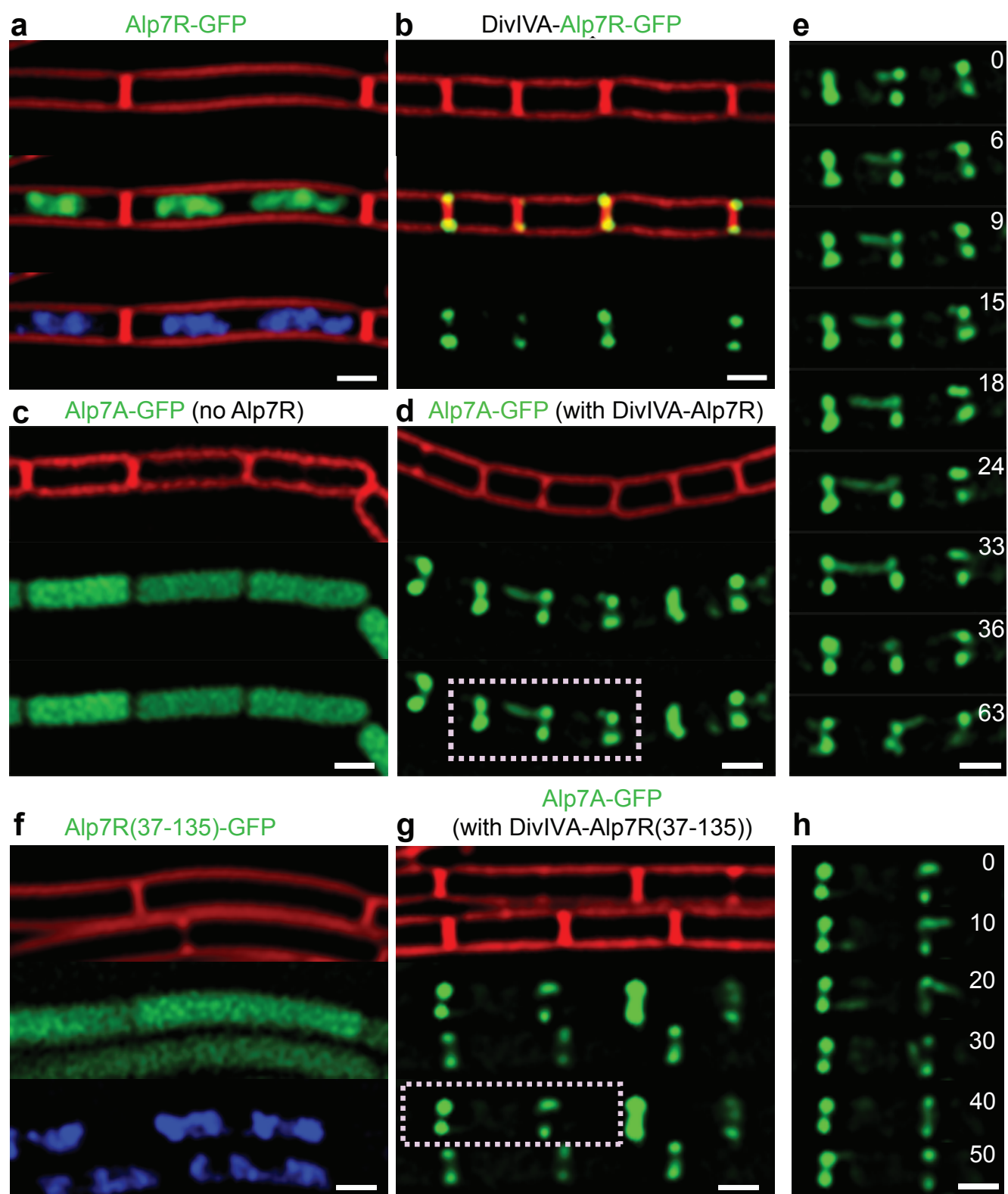
h
0
10
20
30
40
50
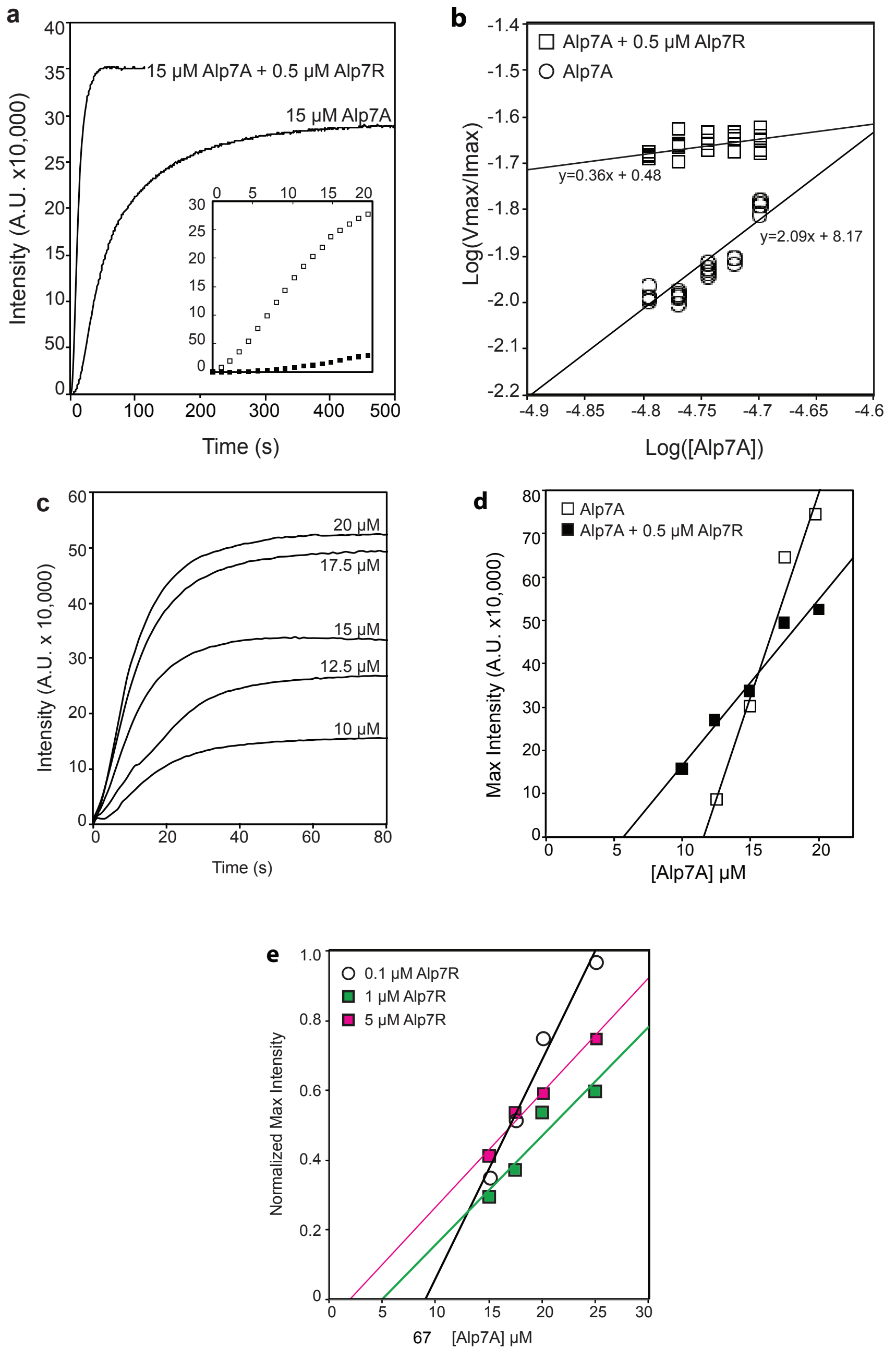
Figure 3: Alp7A is highly dynamic and forms ephemeral filaments well below the dynamic critical concentration in the absence of Alp7R
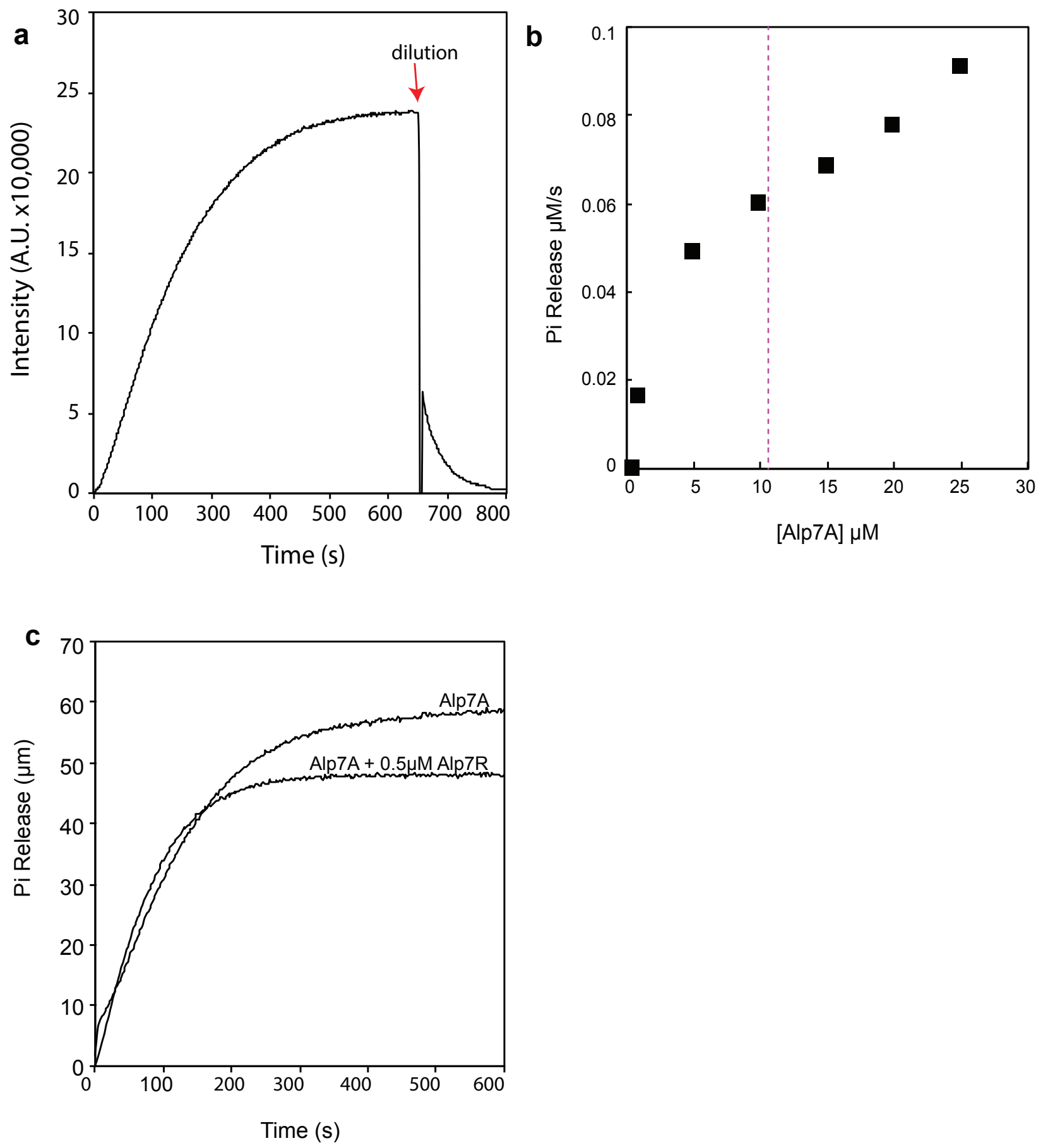
Figure 5: Alp7R depresses the critical concentration of Alp7A by stabilizing highly ephemeral filaments
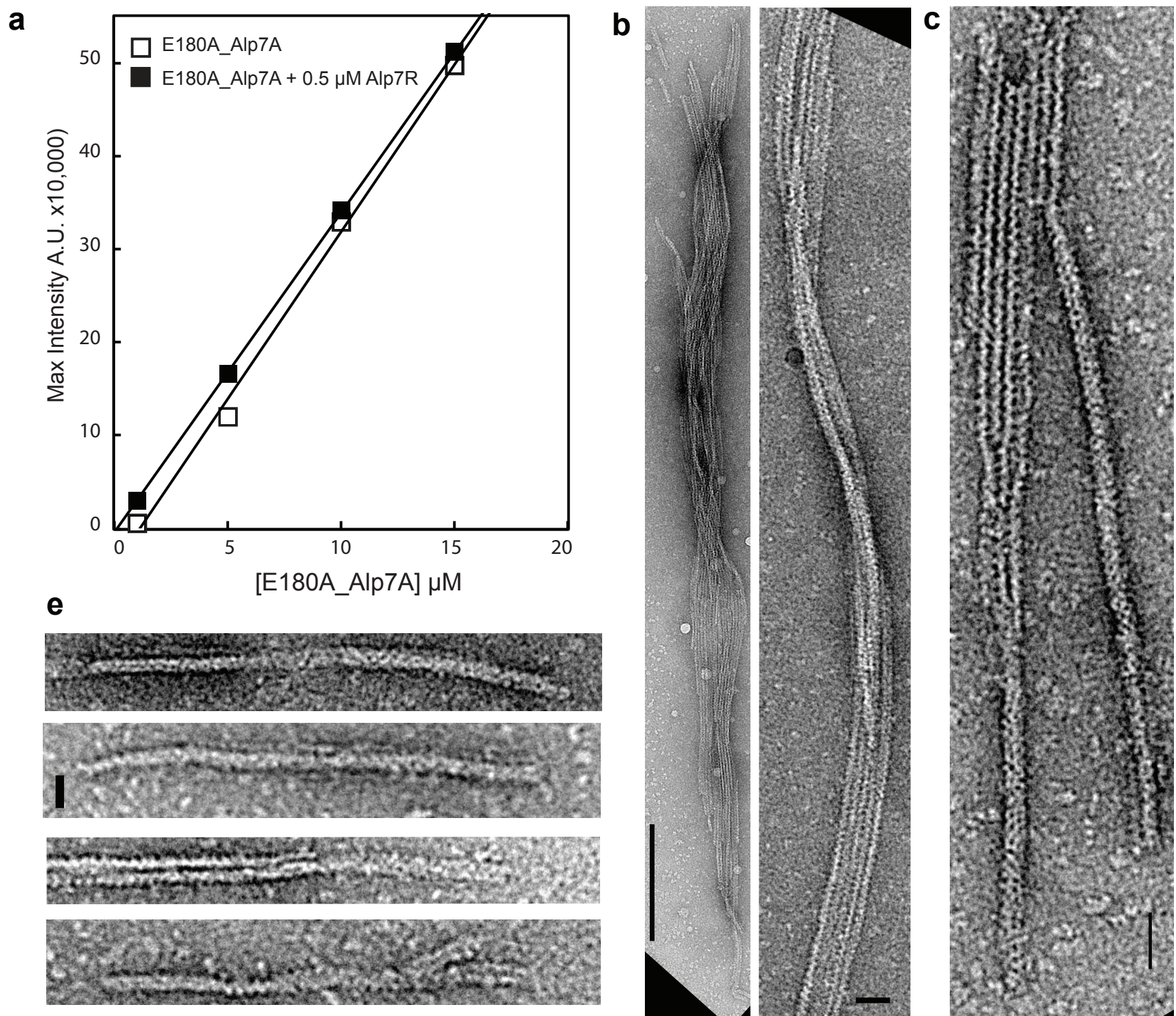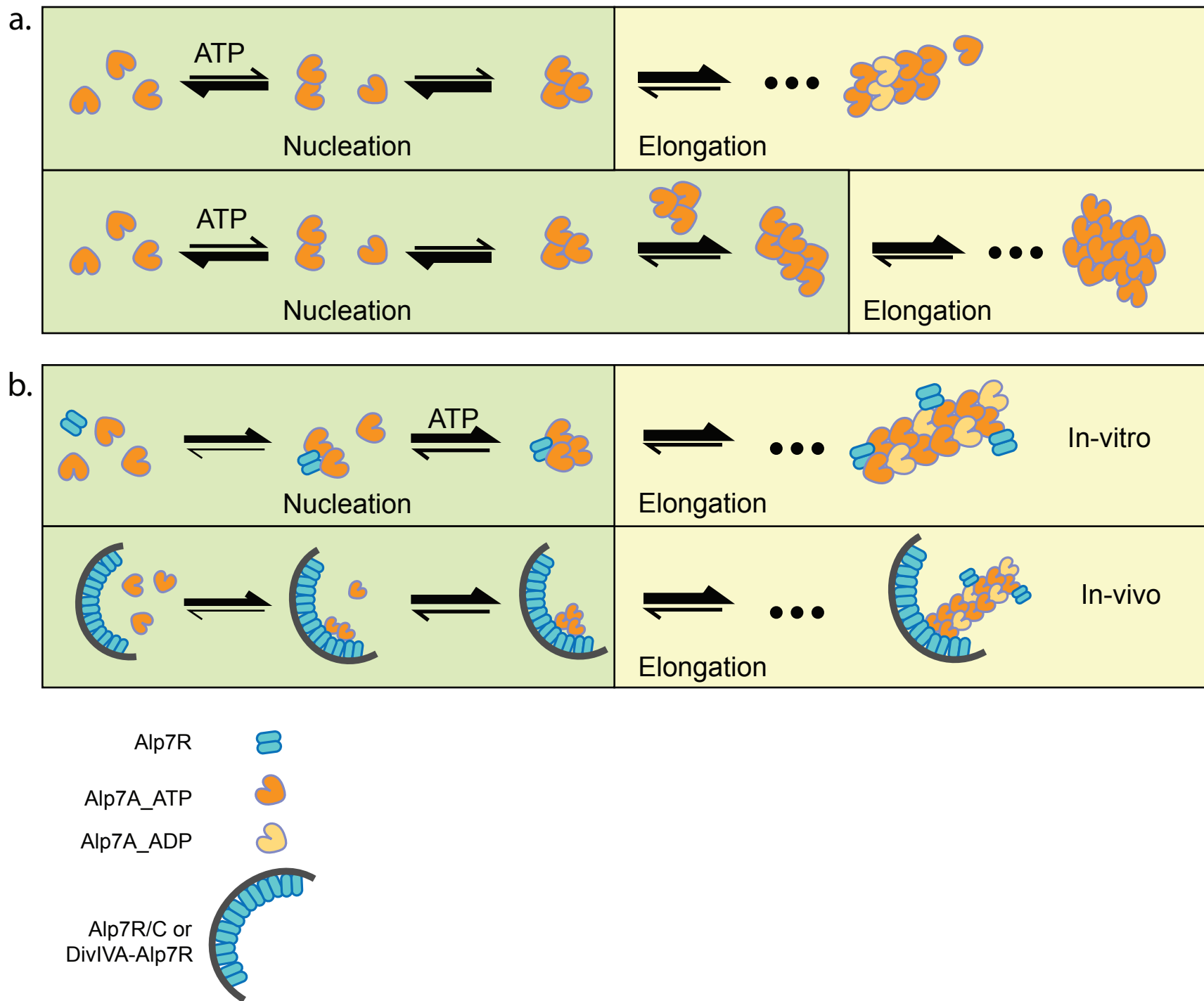
Figure 5: Models of nucleation

Chapter 4:

Nucleotide dependent conformation changes in Alp7A and ParM.

Hydrodynamic approaches shed light on commonly sampled solution states.

Natalie A. Petek, Daniel Elnatan, Karen Cheng, Karen Ruiz, Aditya Anand, Xioawei Yan,

David A. Agard, R. Dyche Mullins

INTRODUCTION:

As discussed in chapter 1, actins and actin-like proteins are typically described as being closed in the nucleotide-bound state and open in the nucleotide-free state. Closure is a result of a conformational rearrangement of domain II/IB in actin/alps respectively upon nucleotide-binding. Alp7A has a uniquely low affinity for binding nucleotide triphosphates (NTPs), and we hypothesized that this could be in part due to it's relatively open ADP-bound state. Our attempts to crystalize Alp7A in the absence of nucleotide or with non-hydrolyzable ATP/GTP failed. In the absence of high resolution structural information of multiple nucleotide-binding states for Alp7A we turned to bead-modeling, analytical ultracentrifugation (AUC) and small angle x-ray scattering (SAXS) to understand if Alp7A shared this fundamental actin characteristic. We used ParM from the R1 plasmid as a proof of principle since many nucleotide states have been crystalized. We use bead models to predict the trends in conformation-dependent change in sedimentation coefficients, and observe the same trend in solution. Our predicted sedimentation coefficient for ADP-bound Alp7A closely matches the AUC measurement, and reveals that ALp7A likely undergoes a significantly larger rearrangement than that of ParM. SAXS data in the absence and presence of nucleotide demonstrate that Alp7A is in a more closed state in the presence of ADP.

RESULTS:

We observed in our purifications of Alp7A that it elutes from a gel filtration column (superdex 200) in two discrete peaks (figure 1). This is a well described phenomena for eukaryotic actin, the first peak being a higher molecular weight pool of small oligomers and the second peak being the monomeric fraction. However for Alp7A, we observed that the 'oligomeric peak' did not have any nucleation activity by right angel light scattering as would be expected for small oligomers (data not shown). We therefore hypothesized that these two peaks could instead be a nucleotide-free state (peak 1), and a nucleotide-bound state (peak 2). This could be possible if the stokes radius of Alp7A is sufficiently different for the two states. To determine what --if any-- oligomeric species where present in peak 1, we performed sedimentation equilibrium experiments of freshly eluted fractions from the left shoulder of peak one (Figure 1, blue stripe). At three rotor speeds equilibrium traces at three different concentrations fit best to a single, non associating species at approximately 45 kDa (Figure 2). This result demonstrates that both Alp7A peaks are monomeric since the molecular weight of Alp7A is 44815.1 kDa, and suggests that more than one conformational state of Alp7A is present in solution.

To test whether this conformational rearrangement is nucleotide dependent, we turned to analytical ultracentrifugation. In order to determine whether this was a viable method for measuring nucleotide dependent closure we first looked at ParM from the R1 plasmid, primarily because high resolution crystal structures of the Apo (nucleotide-free) and ADP-bound state of the protein have been solved (Figure 3A). In the ADP-bound state (1MWM), ParM is considered closed, with a S9->T174 distance of 8Å, whereas this distance is 10.9Å in the apo state (1MWK). Bead models of ADP-bound and Apo ParM generated using hydropro software(Ortega

et al, 2011) predict a sedimentation coefficient of 3.08 and 2.98s respectively (Figure 3B), suggesting that we should be able to measure the change in sedimentation coefficient upon nucleotide binding. Sedimentation velocity experiments in the presence or absence of 200 μM ADP (n=3+) determined the sedimentation coefficient to be 3.10s and 2.97s respectively. While the shift towards a smaller, faster migrating species in the nucleotide bound state matches with the theoretical data, the shift was greater than expected. The experimental and theoretical sedimentation coefficients matched well for the apo state, however the nucleotide-bound state migrated slightly faster than expected, suggesting that in solution, ParM-ADP is more compact than in the crystal lattice. Consistent with this idea, a bead model of the ParM-AMP-PNP crystal structure (4A62) had a predicted sedimentation coefficient of 3.10s, which matched the experimental measurement.

We next tested whether we could detect a nucleotide dependent conformational rearrangement of Alp7A. A bead model of the Alp7A-ADP (5EC0) crystal structure predicted a sedimentation coefficient of 3.52s (Figure 3C). Our measured value for Alp7A-ADP sedimentation coefficient is 3.47, while strikingly the APO sedimentation coefficient is 3.10s. This is consistent with a closing of Alp7A upon nucleotide binding, however the change in sedimentation coefficient is much greater than would be expected. Alp7A is approximately 9 kDa larger than ParM which makes it surprising that the APO state of Alp7A would sediment at the same rate as ADP-ParM. Bead models made by separating Alp7A into two lobes and moving them with respect to one another (Figure 3D) failed to reproduce dramatic change in sedimentation coefficient.

To corroborate these data, we performed SAXS on ParM and Alp7A in the presence and absence of ADP. Consistent with the AUC data we see a global shift toward shorter interatomic distances in the presence of ADP for both ParM (Figure 4A) and Alp7A (Figure 4B). The shift towards a more 'closed' conformation is greater for Alp7A than ParM which mirrors our AUC results. We were able to generate bead models from our Alp7A data sets (Figure 4C) which predict sedimentation coefficients of 3.24 for the ADP-bound and 3.16 for the APO Alp7A.

thesis **METHODS**:

Purification of Alp7A: is described in Chapter 2.

Purification of ParM: was performed as described by (van den Ent *et al*, 2002)

Analytical ultra centrifugation:

For sedimentation equilibrium experiments, Alp7A was gel filtered after polymerization and depolymerization cycling into 25mM Tris pH 7.6, 100 mM KCl, 1mM $MgCl_2$, 1mM DTT. Prior to loading into the cell, Alp7A was centrifuged in a TLA 100.4 rotor at 80,000 rpm for 20 minutes to remove aggregate. Protein was diluted to an A_{280} of 0.15, 0.3 and 0.6. Samples were loaded into a 6-well chamber, placed in a rotor (model An-60; Beckman Coulter), and spun at three dif- ferent speeds (e.g., 7, 10, and 14 K rpm) in an ultracentrifuge (16–20 h per speed; model XL-I; Beckman Coulter). Continuous scans were acquired every 2 h at 280 nm to monitor the sedimentation of native Alp7A. Global fitting of three equilibrium traces (e.g., 7K, 10K, 14K rpm) for each condition was performed using NIH Sedphit and Sedphat software(Schuck, 2000).

For sedimentation velocity experiments: Alp7A-Alexa488 was buffer exchanged into 25mM Tris pH 7.6, 100mM KCl, 1mM MgCl2, 1 mM DTT. ParM-Alexa488 was buffer exchanged into 25 mM Tris pH 7.5, 100 mM KCl, 1 mM MgCl2, 1 mM DTT. After buffer exchange protein was centrifuged at 80K rpm in a TLA 100.2 rotor for 20 min. Protein was loaded into 2-channel cells, or meniscus-matching cells and blanked against buffer or protein + ligand respectively.

SAXS: Proteins were prepared as described for analytical ultracentrifugation with the exception that unlabeled protein was used. SAXS data were collected at protein concentrations between 5-6

mg/ml at 4ºC using an aluminum cuvette mounted in the liquid cooled sample holder at the

UCSF in-house beamline. Data were processed using yet unpublished scripts developed by

Daniel Elnatan.

REFERENCES:

Ortega A, Amorós D & García de la Torre J (2011) Prediction of hydrodynamic and other

solution properties of rigid proteins from atomic- and residue-level models. *Biophys. J.*

101: 892–898

Schuck P (2000) Size-distribution analysis of macromolecules by sedimentation velocity

ultracentrifugation and lamm equation modeling. *Biophys. J.* **78:** 1606–1619

van den Ent F, Møller-Jensen J, Amos LA, Gerdes K & Löwe J (2002) F-actin-like filaments

formed by plasmid segregation protein ParM. *EMBO J* **21:** 6935–6943

FIGURE LEGENDS:

Figure 1: Alp7A elutes from gel filtration as two peaks

Gel filtration profile of Alp7A after depolymerization. Alp7A elutes as two peaks. The blue bar indicates fractions used for analytical ultracentrifugation in figure 2.

Figure 2: Multi-speed Equilibrium sedimentation reveals that Alp7A "dimer" peak is monomeric

Sedimentation equilibrium of freshly eluted native Alp7A from gel filtration peak 1. Based on a global fit of three concentrations of Alp7A at three rotor speeds each, Alp7A is monomeric in solution. Best fits were obtained with a single species non-associating model, which predicted a molecular weight of 43,000-46,000. Alp7A molecular weight is 44, 815.1. Orange is 7K, Green is 10K and Blue is 14K.

Figure 3: Predicted sedimentation coefficients by bead model

(A) Crystal structures of ParM from the R1 plasmid in the APO (left, 1MWK), ADP (center, 1MWM), and AMP-PNP (right, 4A62). (B) Bead models generated using hydropro software from the crystal structures in 'a.' Theoretical sedimentation coefficients are below each bead model. (C) Crystal structure of Alp7A-ADP with corresponding bead model and theoretical sedimentation coefficient. (D) Alp7A structures generated by rotation of domain IB away from the protein core. Range of sedimentation coefficients predicted by bead models of corresponding structures.

Figure 4: Nucleotide dependent closure of Alp7A by SAXS

(A) Distribution of interatomic distance for ParM in the presence or absence of 200 µM ADP as determined by small angle x-ray scattering. (B) Distribution of interatomic distances for Alp7A in the presence or absence of 20 mM ADP. (C) Bead models of Alp7A-APO (left) and Alp7A-ADP (right). Theoretical sedimentation coefficients are below each model.

Table 1: Experimental and theoretical sedimentation coefficients of ParM and Alp7A

Chart of experimental and theoretical sedimentation coefficients as determined by 2 sedimentation velocity methods as well as bead modeling.

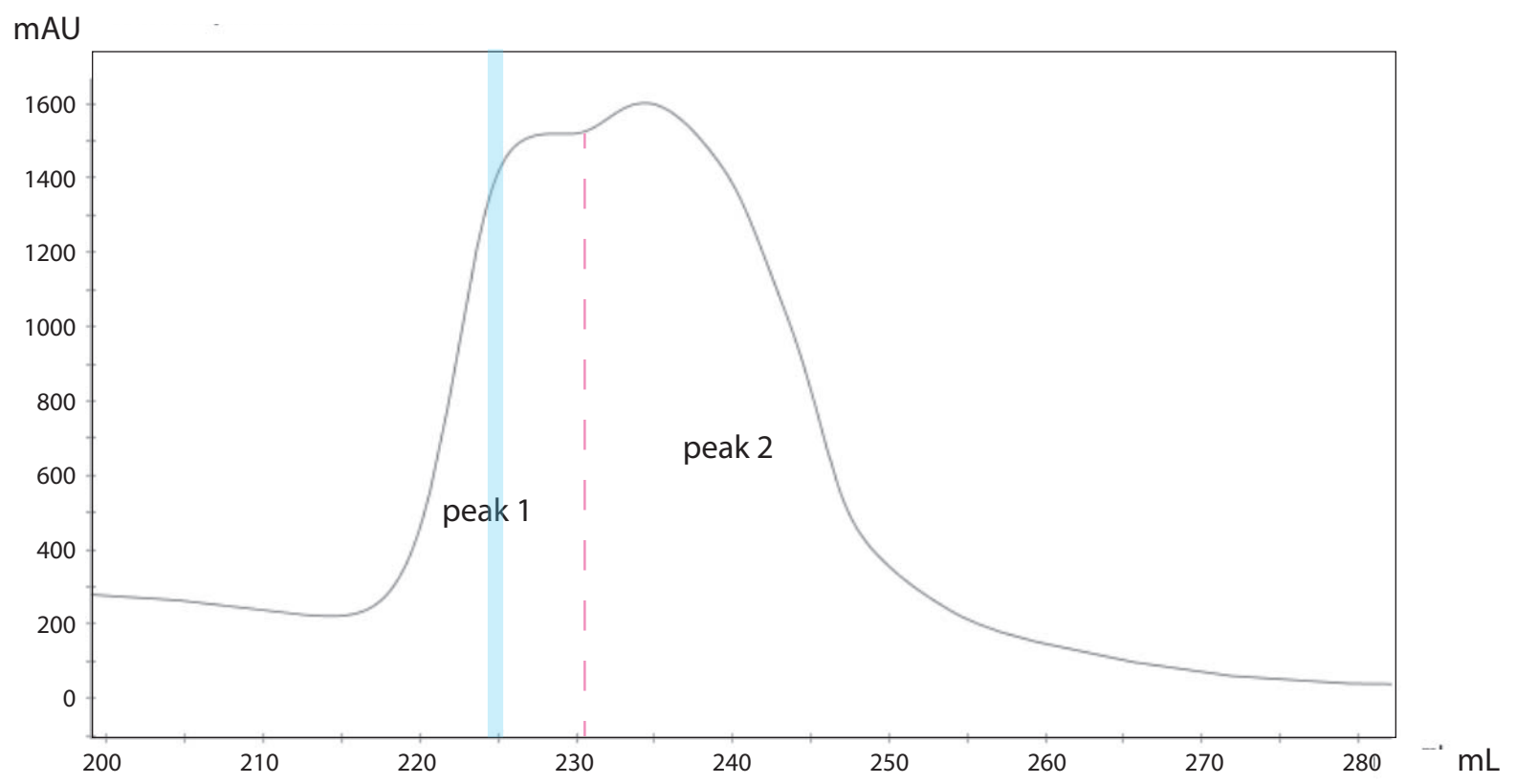Figure 1: Alp7A elutes from gel filtration as two peaks

Figure 2: Multi-speed Equilibrium sedimentation reveals that Alp7A "dimer" peak is monomeric
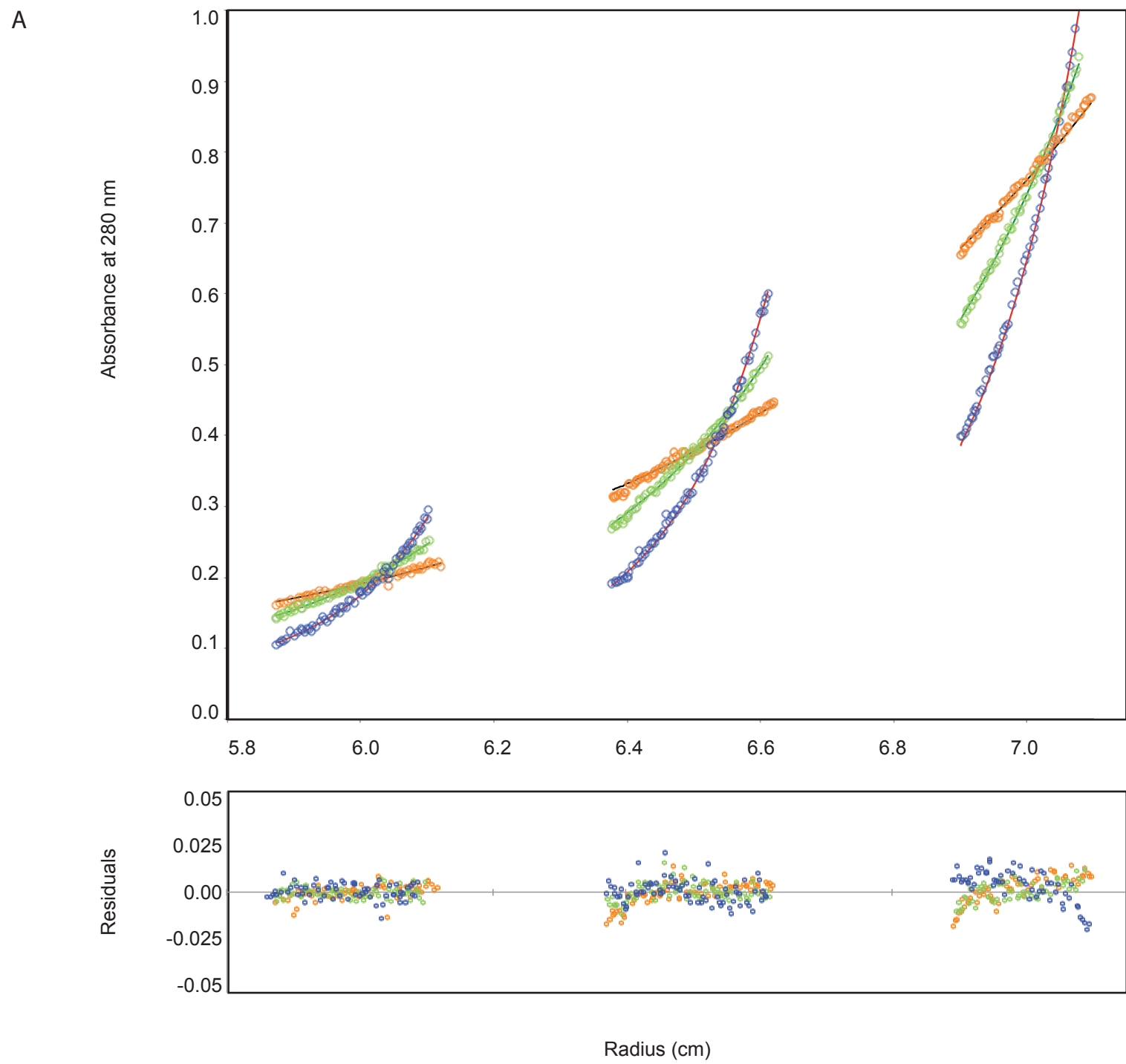
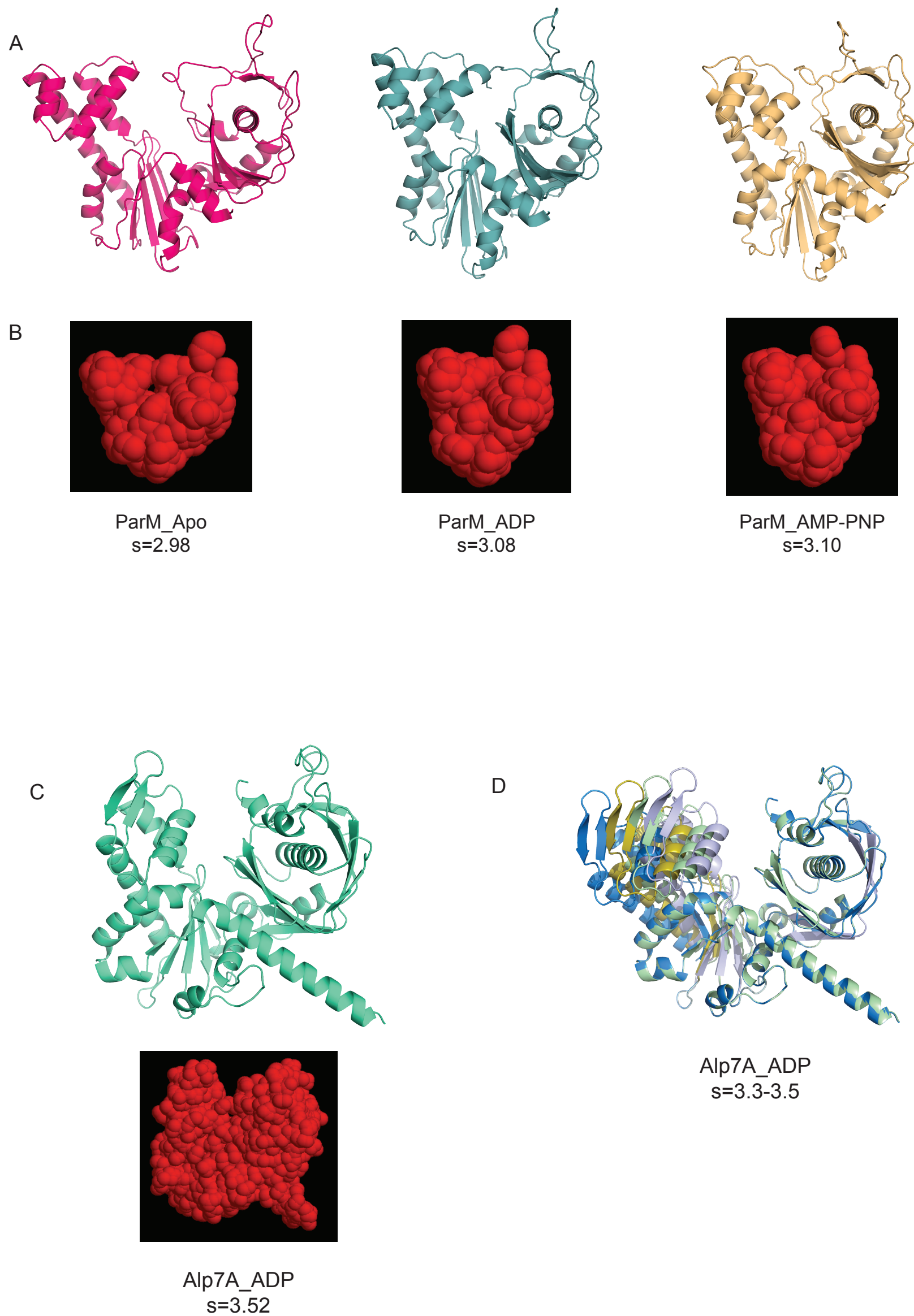Figure 3: Predicted sedimentation coefficients by bead model

A

B

ParM_Apo
s=2.98

ParM_ADP
s=3.08

ParM_AMP-PNP
s=3.10

C

Alp7A_ADP
s=3.52

D

Alp7A_ADP
s=3.3-3.5

Figure 4: Nucleotide dependent closure of Alp7A by SAXS

A   ParM

B   Alp7A

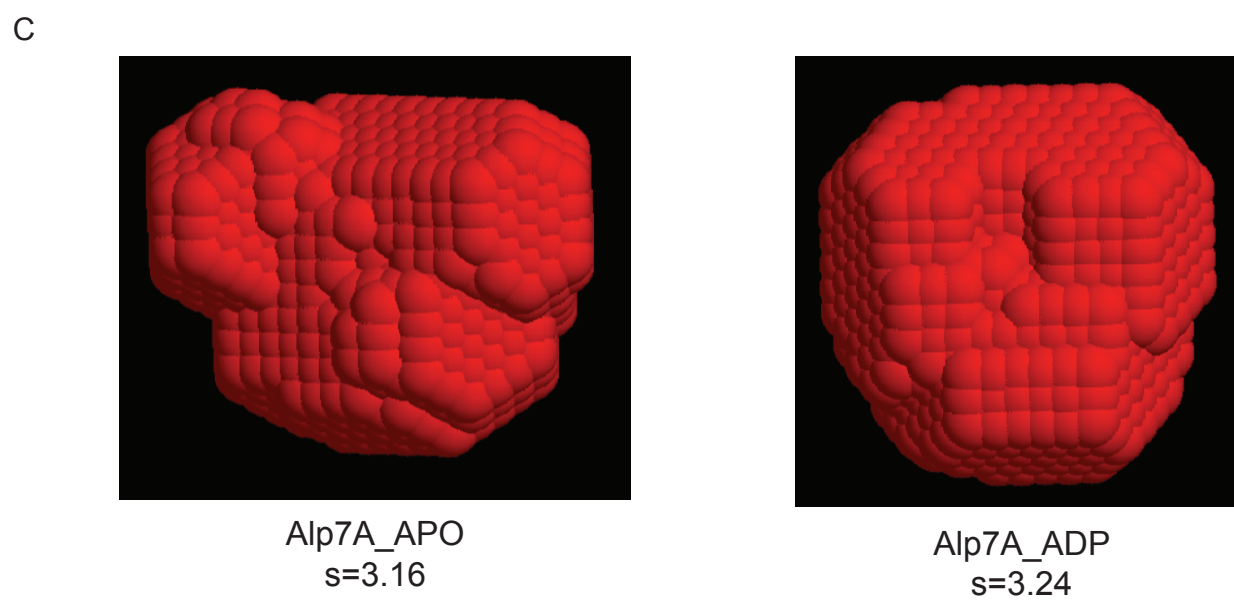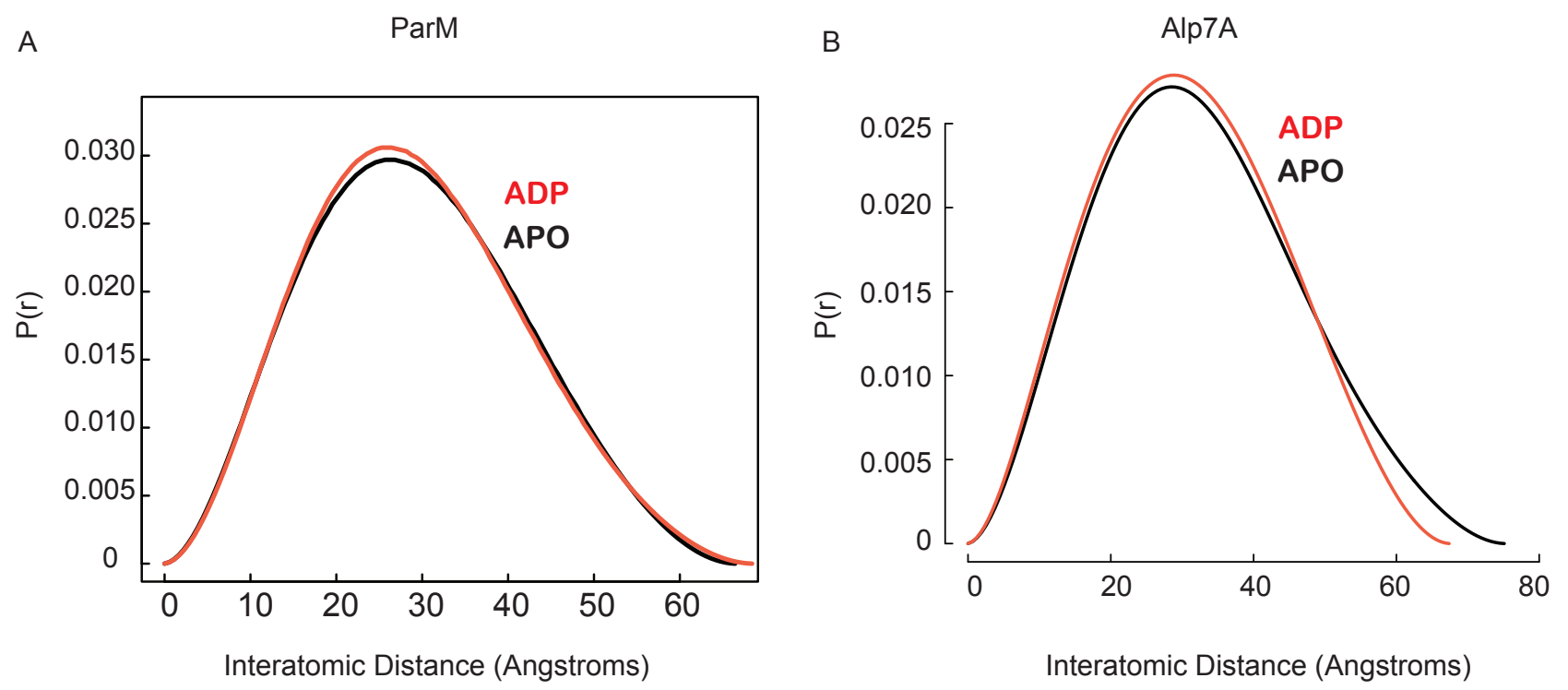C

Alp7A_APO
s=3.16

Alp7A_ADP
s=3.24

Table 1: Experimental and theoretical sedimentation coefficients of ParM and Alp7A

Sedimentation Coefficient	ParM w/o ADP	ParM WITH ADP	Alp7A WITH ADP	Alp7A w/o ADP
AUC	2.97 n=4	3.10 n=4	3.47 n=1	3.1 n=2
AUC Meniscus-matching centerpiece	2.98 n=3	3.09 n=3	-----	-----
Bead Model	2.99	3.08	3.52	n/a

Chapter 5

Conclusion:

The characterization of Alp7A and it's regulation by DNA binding protein Alp7R are a prime example of how studying an exceptionally irregular system can shed light onto the function of well studied ones. When we first purified Alp7A, we were astonished by how bizarre it seemed by comparison to actin and bacterial ALPs. For example, it required <u>vastly</u> higher protein and nucleotide concentrations for polymerization than other know actin-like proteins. It's nucleotide affinity is so poor it is hard to understand how it can function as an ATPase, especially given that according to plasmid stability assays it is the most stable of all known actin-based segregation systems. However, as we learned more about Alp7A --how it was stabilized and nucleated-- we began to realize in retrospect that we seen some of the same behaviors in ParM, and AlfA. For example, similar to Alp7A, ParM also has a range of protein concentrations wherein it forms highly ephemeral filaments, that require stabilization by either interaction with the ParR/C complex, or dare I say it, lateral annealing. This second behavior was one that we saw in reconstitution assays, but did not quite understand. Recent structural studies have provided evidence that ParM requires a pair of antiparallel filaments to form a stable spindle. In retrospect, our reconstitution assays showed antiparallel association of ParM filaments --a property that we ignored at the time, but we now believe to be true. With respect to nucleation, AlfA was described previously as being nucleated by AlfB. As a result of my work on Alp7A/R we now better understand those results. Alp7R <u>is</u> in fact a nucleator of Alp7A filaments; in the absence of Alp7R, five to six kinetically resolvable steps are required for elongation to be favored (a number that we believe reflects the necessity for nuclei to laterally anneal for stability). However

in the presence of Alp7R, there is only one kinetically resolvable step. This is likely because

Alp7R--a dimer-- can bind two Alp7A-ATP molecules forming a pre-nucleus, one additional

monomer will then form a stable nucleus for a two-stranded filament. For AlfA nucleation by

AlfB, the kinetically resolvable steps were altered from four steps to three steps. We know that

AlfB disassociates AlfA bundles (or prevents them from annealing), so it is now clear that this is

NOT nucleation, but instead reflects the nucleation of single two-stranded filaments (three steps)

rather than bundles (four steps). This brings me to the stabilization of dynamic filaments. Alp7A

has helped us to understand that there are two basic mechanisms for how dynamically unstable

actins are stabilized, either through interaction with plasmids (through the DNA binding protein),

or by lateral filament annealing. While we previously believed AlfA to not share the property of

dynamic instability with other ALPs, it is now clear that it is inherently unstable. As a field we

have been leery of calling proteins 'dynamically unstable' unless they share the same mechanism

of dynamic instability as eukaryotic microtubules. However, it is now clear that many

mechanisms exist to inherently destabilize filaments. While the field refuses to acknowledge the

dynamic instability of AlfA, it clearly falls into this category. Mutants of AlfA that are unable to

bundle (or bundle weakly), treadmill, and rapidly disassemble (by comparison to WT AlfA) in

vitro. Lateral annealing is required to stabilize these polymers. We have known that ParM is

dynamically unstable, but not until recently was it clear than filament annealing played a role in

filament stabilization. Now our study of Alp7A shows that there are a core set of principles that

are shared between the ALPs involved in plasmid segregation. Despite their diverse filament

architecture, atomic structures and assembly kinetics, they all display: (1) inherent dynamic

instability (2) stabilization by plasmid complex binding, (3) a propensity to form bundles, which are often antiparallel in nature.
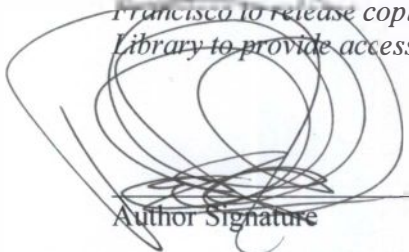
Thus, they aren't so different after all.

Publishing Agreement

It is the policy of the University to encourage the distribution of all theses, dissertations, and manuscripts. Copies of all UCSF theses, dissertations, and manuscripts will be routed to the library via the Graduate Division. The library will make all theses, dissertations, and manuscripts accessible to the public and will preserve these to the best of their abilities, in perpetuity.

Please sign the following statement:
I hereby grant permission to the Graduate Division of the University of California, San Francisco to release copies of my thesis, dissertation, or manuscript to the Campus Library to provide access and preservation, in whole or in part, in perpetuity.

_____ $\underline{3/24/16}$
Author Signature   Date